

INDUCTION MOTOR BEARING FAULT DETECTION
USING A FRACTAL APPROACH

A Thesis

by

JIANXI FU

Submitted to the Office of Graduate Studies of
Texas A&M University
in partial fulfillment of the requirements for the degree of

MASTER OF SCIENCE

December 2010

Major Subject: Mechanical Engineering

INDUCTION MOTOR BEARING FAULT DETECTION
USING A FRACTAL APPROACH

A Thesis

by

JIANXI FU

Submitted to the Office of Graduate Studies of
Texas A&M University
in partial fulfillment of the requirements for the degree of

MASTER OF SCIENCE

Approved by:

Chair of Committee,	Alexander G. Parlos
Committee Members,	Won-Jong Kim
	Bryan Rasmussen
	Jose Silva-Martinez
Head of Department,	Dennis O'Neal

December 2010

Major Subject: Mechanical Engineering

ABSTRACT

Induction Motor Bearing Fault Detection Using a
Fractal Approach. (December 2010)

Jianxi Fu, B.S., Tsinghua University, Beijing, China

Chair of Advisory Committee: Dr. Alexander G. Parlos

Fault detection is an important research area in mechanical engineering. Literature surveys indicate that bearing failures are considered the most common failure modes in motors. Various faults related to bearings can be categorized into single-point defects or generalized roughness defects. In many research studies, monitoring methods based on vibration signals are used to detect single-point bearing failures. Depending on which bearing surface contains the fault, the characteristic vibration frequencies can be calculated from the rotor speed and the bearing geometry. It also has been demonstrated that stator current monitoring can provide the same indication without requiring access to the motor.

The combination of phase space reconstruction and fractal theory may provide an effective approach to detect bearing generalized roughness faults in induction motors by assembling the estimation of dynamic invariant properties of a nonlinear system. In mathematics, a delay embedding theorem gives the conditions under which a chaotic dynamical system can be reconstructed from a sequence of observations of the state of a dynamical system by lagging the time series to embed it in more dimensions. One can

determine the delay time by calculating mutual information with equality distant space cells. False nearest neighbors provides a robust way to determine necessary embedding dimensions. Almost all chaotic systems have a quantifying measurement known as a fractal dimension which is extracted from the original or reconstructed phase space. There are many specific forms of fractal dimension. In this research, correlation dimension is used to estimate the dimension of attractors in nonlinear dynamical systems.

Taking the result of Fourier based analysis as a reference for fault detection, experimental results show that the proposed method is as effective in detecting bearing generalized roughness faults in induction motors.

To My Parents and Brother

ACKNOWLEDGEMENTS

I would like to express my appreciation to my committee chair and advisor, Dr. Alexander G. Parlos, for his patience, continuous guidance, technical support and advice through the course of my research work. I would also like to express my appreciation to other members of my committee: Dr. Won-Jong Kim, Dr. Bryan Rasmussen and Dr. Jose Silva-Martinez, for their comments and advice.

Thanks also go to the Veros Systems Inc., which provided the survey instrument, and to Mr. Yong Li who had done two experiments and provided me the data. I also want to extend my gratitude to my friends Mr. Gang Li, Mr. Tengxi Wang and Mr. Pang-Chun Chu at Texas A&M University for their insightful discussions on related and unrelated topics.

Finally, thanks to my parents and brother for their encouragement, patience and love.

TABLE OF CONTENTS

	Page
ABSTRACT	iii
ACKNOWLEDGEMENTS	vi
TABLE OF CONTENTS	vii
LIST OF FIGURES.....	ix
LIST OF TABLES.....	xii
CHAPTER	
I INTRODUCTION.....	1
A. Research Motivation.....	1
B. Literature Review	3
C. Problem Definition and Research Objectives.....	8
D. Proposed Approach.....	8
E. Research Contributions.....	11
F. Thesis Organization.....	11
II PROPOSED BEARING FAULT DETECTION METHOD.....	13
A. Phase Space Reconstruction	13
1. Embedding Lag	17
2. Embedding Dimension	21
B. Fractal Dimension.....	24
1. Similarity Dimension	28
2. Box-Counting Dimension	31
3. Correlation Dimension	38
4. Influencing Factors on the Correlation Dimension	42
C. Summary of Faulty Detection Algorithm	44
III EXPERIMENTAL SETUPS FOR IN-SITU BEARING DAMAGE...	46
A. In-situ Bearing Fault.....	46
B. Shaft Current Experimental Setup.....	48

CHAPTER	Page
IV	EXPERIMENTAL RESULTS..... 53
	A. Induction Motor G563 Loaded by a Blower 53
	1. Vibration Signal Analysis..... 54
	2. Current Signal Analysis..... 56
	B. Induction Motor 3KX07G Loaded by a Generator 58
	1. Vibration Signal Analysis..... 59
	2. Current Signal Analysis..... 61
	C. An Extended Application..... 63
V	SUMMARY AND CONCLUSIONS 65
	A. Summary of Research 65
	B. Conclusions 68
	C. Suggestions for Future Work..... 68
	REFERENCES..... 71
	VITA..... 74

LIST OF FIGURES

FIGURE		Page
1	Reasons for induction motor failure.....	2
2	Bearing faults categorization.....	3
3	Rolling element bearing geometry	4
4	Overall approach of proposed research.....	10
5	Time series and phase space for the Lorenz dynamical system	14
6	Lorenz attractor and reconstruction of the attractor	15
7	Rosler attractor and reconstruction of the attractor.....	16
8	Mutual information value versus time delay τ	19
9	Reconstructed phase space for τ value 1, 2, 3, and 4.....	20
10	False nearest neighbor	22
11	Real nearest neighbor	22
12	Percentage of false nearest neighbor for the Lorenz system	24
13	Sierpinski Triangle	25
14	Segmental coast of Britain	26
15	Measuring the length of a coastline using rulers of varying lengths.....	27
16	Geometric construction of the Sierpinski triangle.....	30
17	How the curve is recursively constructed	31
18	Covering the Sierpinski triangle with smaller and smaller boxes	33
19	Log-Log plot to estimate the box-counting dimension	35

FIGURE	Page
20 Box-counting dimension estimation of the Koch Curve	36
21 Box-counting dimension of coastline of Britain	37
22 Box-counting dimension of Barnsley Fern	37
23 Correlation dimension of Lorenz system	41
24 Correlation dimension of Rossler system.....	42
25 Correlation dimension imposed with different levels of white noise.....	44
26 Summary of faulty detection algorithm	45
27 Created capacitor within a bearing.....	47
28 Use a shaft current to generate online, in situ bearing faults	48
29 Experimental setup of the motor test-bed	49
30 Vibration signal data acquisition system.....	50
31 Electric signal data acquisition system.....	51
32 An example of socket APIs used for iterative server design.....	52
33 Experimental setup for G563 induction motor loaded by a blower	54
34 Average mutual information and embedding dimension	55
35 Correlation dimension based on vibration data analysis.....	55
36 Average mutual information and embedding dimension	56
37 Correlation dimension based on current data analysis.....	57
38 Average mutual information and embedding dimension	59
39 Correlation dimension based on vibration data analysis.....	60
40 Average mutual information and embedding dimension	61

FIGURE	Page
41 Correlation dimension based on current data analysis	62
42 Correlation dimension based on field analysis.....	64

LIST OF TABLES

TABLE		Page
1	Computed similarity dimension of objects.....	29
2	Calculate the occupied boxes of each grid-size	34
3	Computational results of correlation dimensions with different sample size.....	43

CHAPTER I

INTRODUCTION

A. Research Motivation

Induction motors are often in a critical role in industrial processes and are the most popular because of their simplicity of construction. Like all rotating machinery, reliability of induction motors is not 100%. Arranging a schedule for motor maintenance plays a very important role in modern industry. An inadequate maintenance plan may lead to significant losses as a result of shutdown times or an accidental breakdown of motors that result in bigger losses. The condition based maintenance (CBM) strategy is assessed as the most effective technology that moves the maintenance effort from a scheduled, preventative format to a more flexible and accurate condition based predictive format [1].

Fault detection, which is a very important research area in mechanical engineering, has significant role within a CBM system. By spotting fault sources and making maintenance proactive before any failure occurs, a CBM system keeps operators up to date on how motors are performing, helping avoid any loss from deviations from expected normal performance. Therefore a CBM system can access and estimate machine condition, enabling maintenance to be performed proactively, rather than reactively. The main aims of machine fault detection are to minimize unplanned down-

This thesis follows the style of *IEEE Transactions on Automatic Control*.

time while enabling safe, and to optimize motor performance under all operating conditions.

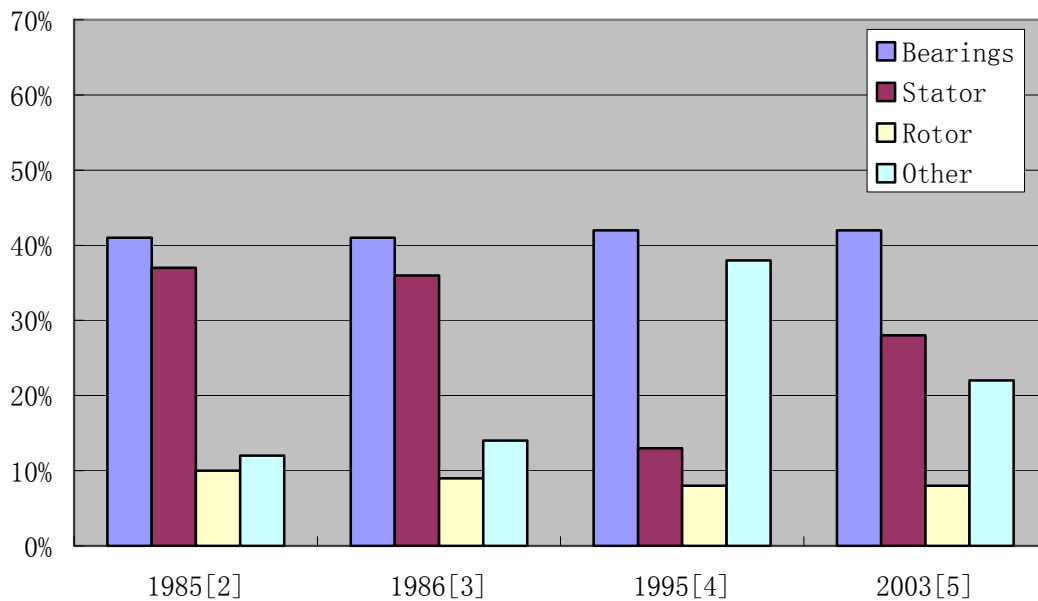


Figure 1. Reasons for induction motor failure.

Typical failures of an induction motor can be classified into bearing, stator, rotor, and other failures. Figure 1 presents a summary of the main reasons for induction motor failures. According to O'Donnell [2] and Albrecht [3] 41% all failures of electric motors in 1985 and 1986 were related to bearings. Furthermore, some similar studies on the major component failure of motors has been conducted by Thorsen [4] and IEEEIGA [5] in 1995 and 2003, bearing faults also have been shown to be the most frequent faults in induction motors. Based on these studies, bearing failures can thus be considered the most common failures of induction motors. Therefore there is a strong motivation to

study bearing faults and develop a method for detecting faults in induction motor, in general.

B. Literature Review

There are many reasons for bearing failures: wrong or aged lubricant, bearing dirt, inadequate or too much grease, wrong alignment, bearing currents and so on. All faults related to bearing can be categorized into single-point defects or generalized roughness as shown in Figure 2[6]. The convenience of this classification is that it is easy to design different fault detection schemes for such special faults.

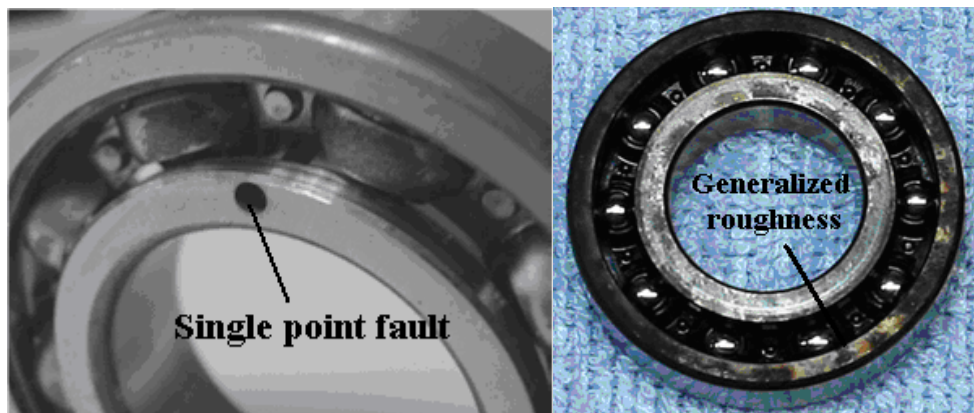


Figure 2. Bearing faults categorization.

A single-point defect is a pit or spall on a bearing surface. Depending on which bearing surface contains the fault, the characteristic vibration frequencies can be calculated from the rotor speed and the bearing geometry [7], as detailed below.

The single-point defect on outer race frequency is given by:

$$f_{outer} = \frac{n}{2} f_{shaft} \left[1 - \frac{D_{ball}}{D_{pitch}} \cos \alpha \right], \quad (1.1)$$

the single-point defect on inner race frequency is given by

$$f_{inner} = \frac{n}{2} f_{shaft} \left[1 + \frac{D_{ball}}{D_{pitch}} \cos \alpha \right], \quad (1.2)$$

the single-point defect on ball frequency is given by

$$f_{ball} = \frac{D_{pitch}}{D_{ball}} f_{shaft} \left[1 - \left(\frac{D_{ball}}{D_{pitch}} \cos \alpha \right)^2 \right], \quad (1.3)$$

the single-point defect on train frequency is given by

$$f_{train} = \frac{1}{2} f_{shaft} \left(1 - \frac{D_{ball}}{D_{pitch}} \cos \alpha \right), \quad (1.4)$$

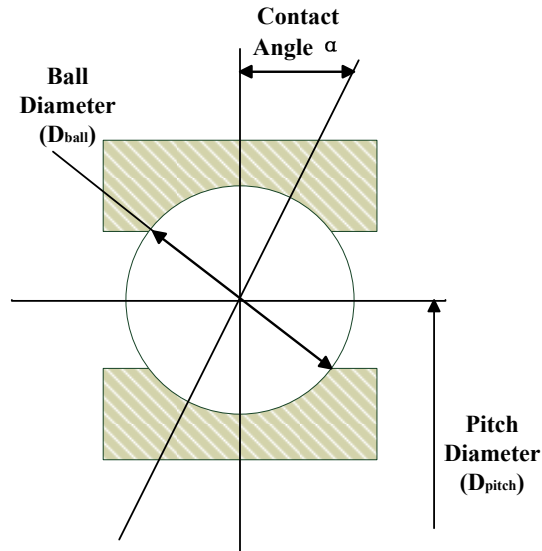


Figure 3. Rolling element bearing geometry.

where D_{pitch} is the bearing pitch diameter, D_{ball} is the ball diameter, n is the ball number,

α is the contact angle of the balls on the races in Figure 3, and f_{shaft} is the mechanical rotor speed in Hertz.

In many studies monitoring methods based on vibration signals are used to detect the single-point bearing failure. Accelerometers are the most common vibration sensors. However, they are expensive and their installations are critical and not justified for every electric machine. It has been shown by Schoen and Habetler that stator current monitoring can provide the same indications without requiring access to the motor [7]. Current-based monitoring techniques usually do not require additional sensors (sensorless) and have great economic benefit for low-cost implementations.

Current-based bearing fault detection is to extract fault signature from the motor stator current. The basic idea of the relationship of bearing vibration to stator current spectrum is the fact that dynamic eccentricity varies with rotor position, and the oscillation in the air gap length causes variations in the air gap flux density. This, in turns, affects the inductances of the motor produced stator current harmonics.

The characteristic current frequencies, f_{cf} , due to the bearing characteristic vibration frequencies, f_v , are calculated by [7]

$$f_{cf} = |f_e \pm m \cdot f_v|, \quad (1.5)$$

where $m = 1, 2, 3, \dots$ and f_e is the power line frequency. As a result, this equation represents that the predictable frequency components typically appear in the machine vibration and are reflected in the stator current.

In fact, there is a lot of literature focusing on the detection of single-point bearing

faults. Conventionally, the Fourier transform gives a good analysis for stationary signals. However, it is well known that Fourier transform analysis exhibits several weaknesses when it is applied to non-stationary signals, since the frequency content of a response varies with time, and ‘averaging’ over a large number of data windows smears the response characteristics. Moreover, the input signals must contain a frequency spectrum rich enough to contain the structural frequency components of interest. Especially when the feature components are weak in magnitude, the desired feature components needed for analysis are difficult to be identified.

To overcome this, the Short Time Fourier Transform (STFT) and Wigner-Ville distribution (WVD) have become popular methods for non-stationary signal analysis. Yazici and Kliman used an adaptive statistical time-frequency method for detection of broken bars and bearing faults in motors using stator current [8]. More recently, the wavelet analysis is also increasingly applied to this problem. Eren and Devaney have successfully detected bearing damage via wavelet packet decomposition of the stator current in [9].

In contrast to single-point defect, generalized roughness is defined when bearing surface has degraded over a large area and has become rough or deformed. The generalized roughness is difficult to predict, because these faults are not observable at the early stages. Such faults may cause broadband changes in the stator current and may increase machine eccentricity level. In single point defect of bearing faults, the fault related frequencies can be detected according to the bearing geometry dimensions, while the characteristic fault frequencies for the current or vibration associated with this type

of generalized roughness bearing faults are residing in wide frequency bands and are not easily detectable or predictable.

Most single-point bearing fault detection techniques mentioned above are based on locating and processing the characteristic fault frequencies in vibration and stator current. They are not suitable for detecting generalized roughness faults. The mean spectral deviation (MSD) method in [10] is used to detect generalized roughness faults, but it has some disadvantages. First, it requires thorough knowledge of stator current spectrum distribution to design a set of notch filters used to eliminate non-bearing fault components. Second, it assumes that the components at the frequencies to be eliminated do not contain fault information, which may not be true in practice. Third, machine speed must be measured or estimated. And L. Wang has successfully demonstrated that both bispectrum estimation and Amplitude Modulation Detector (AMD) can be used for generalized roughness fault detection in his research [11]. However, these analysis are be done in traditional frequency domain.

Fractal analysis has now become widely used to interpret variable and unpredictable physical phenomenon, and have obtained substantial results in image and signal processing. Chih-Hao Chen and Rong-Juin Shyu diagnose rotating machines using wavelet packets-fractal technology and neural networks in [12]. Logan and Mathew have used the correlation dimension for vibration fault diagnosis of rolling element bearing in [13]. The application of current- based fractal analysis to bearing fault diagnosis in induction motors is still in its early stages. Further work is needed to investigate exact effects.

C. Problem Definition and Research Objectives

From the previous sections, it can be inferred that it would be desirable to develop a method for detecting induction motor and/or driven load faults while eliminating some of the drawbacks of the existing methods. The objectives of this research are as follows:

- Develop a fault detection method based on the fractal analysis of an underlying dynamic system with unknown dynamic models; assume the availability of input and output measurements only;
- The method must be insensitive to varying operating conditions while being sensitive to fault conditions;
- The method must be applicable to both electrical and mechanical measurements, i.e. current and vibration signals.

D. Proposed Approach

Machine condition monitoring and fault detection present many challenges in the extant literatures, finding an excellent method of fault detection is the key to enable a CBM system to be more useful in practical applications.

In mathematics, a delay embedding theorem gives the conditions under which a chaotic dynamical system can be reconstructed from a sequence of observations of the state of a dynamical system by lagging the time series to embed it in more dimensions. And the reconstructed attractor is the same as that of the real attractor since the spectra are invariant under a smooth coordinate change.

It can be noted that there are two important parameters to reconstructing phase space

from a signal: embedding lag and embedding dimension. Therefore, the first two steps of this research are to find methods to determine values of these two parameters.

Though phase space reconstruction provides a method how to extract the high dimensional feature vector from the measured data, there still one key question: how to indicate the state of reconstructed attractor in order to estimate and forecast the machine health condition. This thesis applies the fractal dimension as an indicator number in evaluating the states of machine health condition. Fractal dimension, developed by the non-linear dynamic and chaos theory, is a promising new tool to interpret observations of physical systems where the time trace of the measured quantities is irregular. Fractal dimension can extract some physically interesting and useful features from such signals, which are generic in non-linear dynamical systems. Fractal dimension has many specific forms, such as the similarity dimension, box-counting dimension, and correlation dimension. It should be taken in full consideration that which dimension is finally used to estimate the dimension of attractors of dynamical systems.

In order to develop a bearing fault detection method, bearing fault data must be acquired before being applied in prognosis. This data is come from two experiments which were finished by other students in previous research. In these experiments, both the non-stationary mechanical (vibration) and electric (voltages/currents) signals for each motor were measured. Especially, the bearing fault data was not created off-line. That is, to disassemble the bearing, damage it, and then assemble the machine. It has been demonstrated in [14] that the act of this process significantly alters the current and vibration characteristics of the machine and corrupts the experimental data. In order to

make bearing fault data valid for use in condition monitoring scheme, shaft current bearing damage was conducted to induce and progress a bearing fault in an accelerated timeframe in the experiments. These faults are generated in situ without disrupting the operation of the electric machine. The overall method proposed for use in this thesis is shown in the Figure 4.

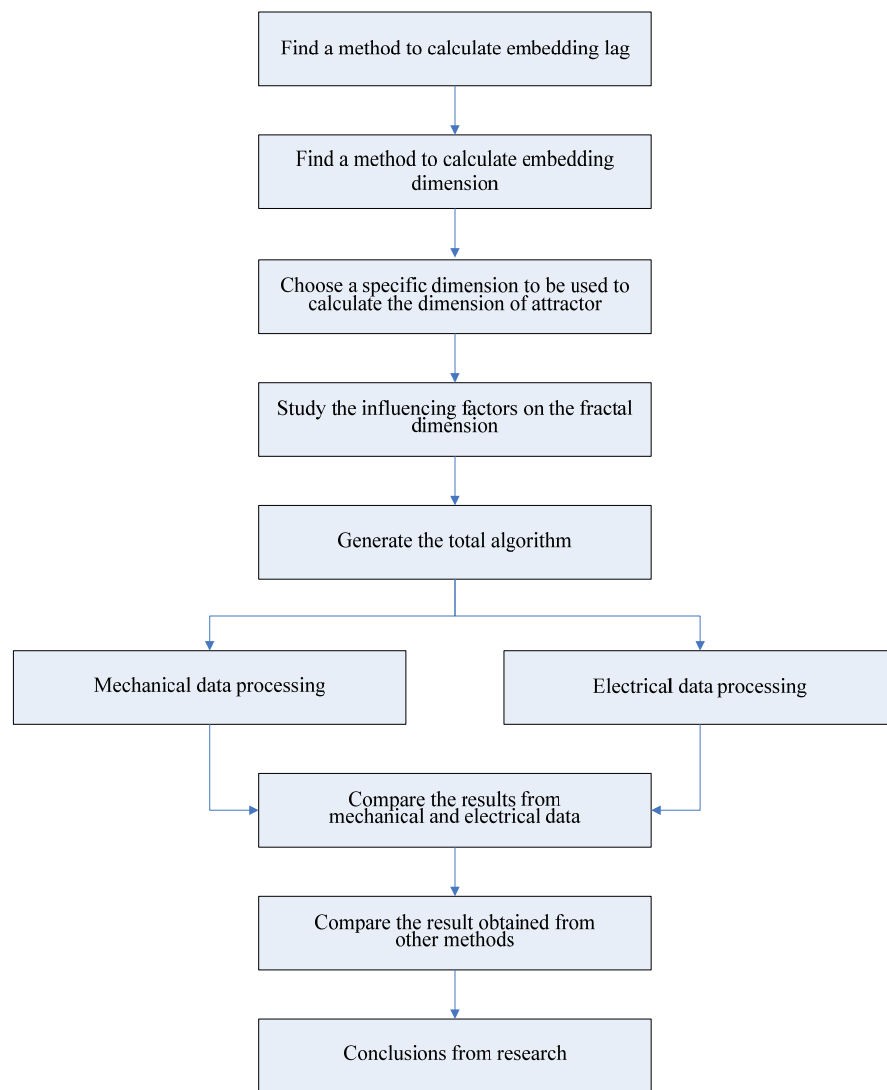


Figure 4. Overall approach of proposed research.

E. Research Contributions

The main contribution of this research is the development of a method for the detection of generalized roughness faults in induction motor bearings. The algorithm has the following characteristic attributes:

- It can be used with electrical (voltages/currents) or mechanical (vibration) measurements;
- Its analytical focus shifts from the frequency domain to a different processing space which is called reconstructed phase space where signal processing techniques are used to extract time-domain based features for signal recognition of faults.
- It uses the correlation dimension as an indicator. The correlation dimension can provide intrinsic information of original dynamic systems from time-series measurements.

F. Thesis Organization

It is expected that this research will provide another method for bearing generalized roughness fault detection in induction motors by using phase space reconstruction and fractal theory. The remaining parts of this thesis are organized as follows. Chapter II presents the analysis in phase space which is different from other approaches in frequency domain. Mutual information and false nearest neighbor methods are used to determine important parameters for space reconstruction. Then some specific forms of fractal dimension are introduced. Correlation dimension is applied to speech detection finally due to its computational simplicity. In Chapter III, faults causes by bearing

current and effects are described. The experimental test bed where the data come from has been established by other students in their previous research. In-situ bearing damage was applied to generated fault data and sets of vibration and electric signal data acquisition are introduced. In Chapter IV, the results of analysis of mechanical and electrical signals from different test beds are presented. To justify the extended application of detecting other fault rather than bearing, the algorithm is also applied to a set of practical data. In Chapter V, a summary and conclusions of this research, and the directions for future work are briefly described.

CHAPTER II

PROPOSED BEARING FAULT DETECTION METHOD

A. Phase Space Reconstruction

Induction motor condition monitoring and health diagnosis present many methods in the extant literatures. Conventionally, motor current signature analysis (MCSA) has been used to estimate the condition of induction motors while the analysis is in the frequency domain [7]. In this thesis, phase space analysis is used as an alternative to these traditional techniques. The analytical focus shifts from the frequency domain to a different processing space where nonlinear/chaotic signal processing techniques are used to extract time-domain based phase space features for speech recognition [15].

In mathematics and physics, a phase space is a space that represents all possible states of a dynamics system. The phase space of a dynamic system can be easily extracted from the equations of motion if this system can be modeled mathematically. The dimension of a system's phase space is the number of degrees of freedom of this dynamic system. Every degree of freedom or parameter of the system is represented as an axis of its multidimensional phase space. With these variables, the system can be completely described. The instantaneous state of a dynamical system is characterized by one unique point in the phase space. A sequence of such states subsequent in time consist a geometric structure emerged in phase space. It is called the attractor of the system.

The Lorenz system is defined by:

$$\begin{aligned}
 \dot{x} &= s(y - x), \\
 \dot{y} &= rx - y - xz, \\
 \dot{z} &= xy - bz, \\
 (s = 10, r = 28, b = 8/3).
 \end{aligned}
 \tag{2.1}$$

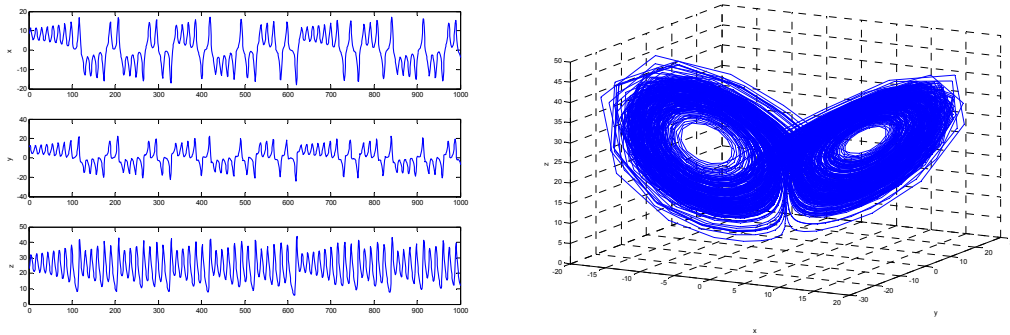


Figure 5. Time series and phase space for the Lorenz dynamical system.

An example of phase space plot for a Lorenz dynamical system is illustrated in Figure 5, and its characteristic attractor is clearly revealed.

Especially for mechanical systems, the phase space usually consists of all possible values of position and momentum variables. It means that the full dynamics of the system are accessible in this space. Because of this, a phase space and fractal dimension extracted from it, which can be found in next chapter for more detail, may potentially contain different information than representation comes from frequency domain.

However, in many practical situations mathematical model of a dynamical system cannot be derived directly. Moreover, it is hard to measure all these variables of a system in most case so that it cannot offer a complete description of the system. Normally, at

least data from one of the system variables can be measured to generate one state time series. In this instance, phase space reconstruction is usually the first step in the analysis of a dynamical system.

Takens' embedding theorem [16] proved that method of time delays provides a relatively simple way of constructing an attractor from a time series of a single component. A copy of the attractor of the system can be reconstructed by lagging the time series to embed it in more dimensions. The embedding theorem states that the dimension and of the reconstructed attractor is the same as that of the real attractor, since the spectra are invariant under a smooth coordinate change [17].

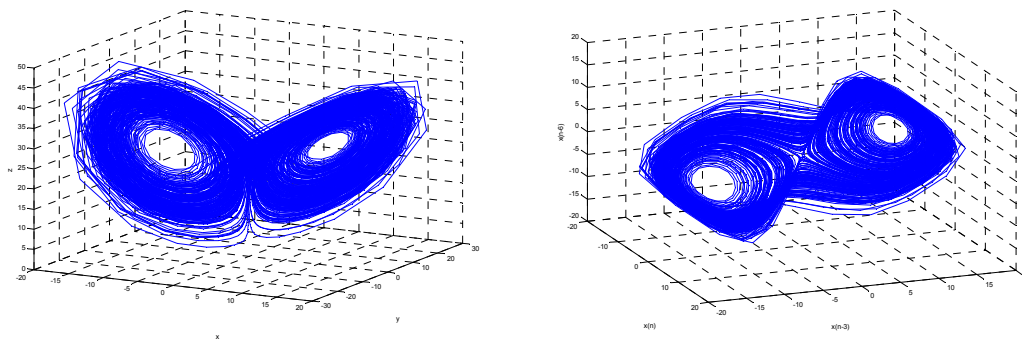


Figure 6. Lorenz attractor and reconstruction of the attractor.

The left panel Figure 6 is a single 5000 point trajectory of Lorenz attractor plotted in x , y and z co-ordinates, the right panel is a delay embedding in three dimensions (embedding lag of 3) of the x co-ordinate. Notice that both original attractor and reconstructed one exhibit two flat and a more complex central region.

Take Rossler system as another example, which is defined by:

$$\begin{aligned}
 \dot{x} &= -y - z, \\
 \dot{y} &= z + ay, \\
 \dot{z} &= b + z(x - c), \\
 (a = 0.398, b = 2, c = 4).
 \end{aligned}
 \tag{2.2}$$

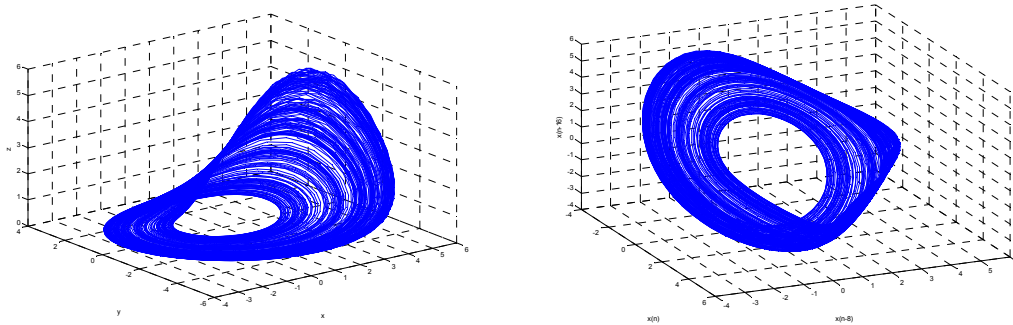


Figure 7. Rossler attractor and reconstruction of the attractor.

The left panel Figure 7 is a single 5000 point trajectory of Rossler attractor plotted in x , y and z co-ordinates, the right panel is a delay embedding in three dimensions (embedding lag of 8) of the x co-ordinate. One can see from both original and embedded co-ordinates that chaos in this system is generated by a gradual stretching apart of trajectories over most of the attractors, combined with rapid folding and compressing at one point.

Therefore, from the previous examples, it can be noted that there are two steps to reconstructing phase space from a signal: first step is choosing a time delay; second step is choosing an embedding dimension.

1. Embedding Lag

Choosing optimum time delay is not trivial and the dynamical properties of the reconstructed attractor are to be amenable for subsequent analysis. The shape of the embedded time series will depend critically on the choice of τ . For smaller values of τ , $s(t)$ and $s(t+\tau)$ will be too closed to each other, so that it cannot supply two independent coordinate or independent variables in dynamic system. It is wise to select a value of τ which separates the data as much as possible. However, for larger values of τ , $s(t)$ and $s(t+\tau)$ will be completely independent of each other, and any connection between them in the case of chaotic attractor is random. Based on analysis above, a criterion is required for intermediate choice that is large enough so that $s(t)$ and $s(t+\tau)$ are independent but not so large that $s(t)$ and $s(t+\tau)$ are completely independent in statistical sense [18].

A competing criterion relies on the information theoretic concept of mutual information, the mutual information criterion (MIC). Determine of delay time by calculating mutual information with equality distant space cells [19]. That means space cells are divided by equal distance step for calculating mutual information, and delay time. This approach is simpler than that of equal probability method [20].

There are two discrete systems $S, \{s_1, s_2, \dots, s_n\}$ and $Q, \{q_1, q_2, \dots, q_n\}$. The mutual information of two discrete random variables S and Q can be defined as:

$$I(S, Q) = \sum_i \sum_j P_{sq}(s_i, q_j) \log_2 \frac{P_{sq}(s_i, q_j)}{P_s(s_i)P_q(q_j)}, \quad (2.3)$$

where $P_{sq}(s_i, q_j)$ is the joint probability distribution function of s_i and q_j , $P_s(s_i)$

and $P_q(q_j)$ are the marginal probability distribution functions of s_i and q_j respectively.

Let $[S, Q] = [X(k), X(k + \tau)]$, determine of delay time by calculating mutual information with equally distance space cells, use provided τ to reconstruction $(x(k), x(k + \tau))$ in (s, q) space, the 2D reconstruction of an attractor is partitioned into a grid of $n \times n$ cells, so the size of each cell in s direction $\varepsilon_s = \frac{S_{\max} - S_{\min}}{n}$, the size of each cell in q direction $\varepsilon_q = \frac{q_{\max} - q_{\min}}{n}$. For every point (s, q) If $(i-1)\varepsilon_s \leq s - s_{\min} \leq i\varepsilon_s$ and $(j-1)\varepsilon_q \leq q - q_{\min} \leq j\varepsilon_q$ are satisfied, that means this point is in the cell ε_{ij} .

The joint probability of occurrence $P_{sq}(s_i, q_j)$ of the attractor in any particular box is calculated by counting the number of discrete points $N_{sq}(i, j)$ in the cell ε_{ij} and dividing by the total number of points on the attractor trajectory.

$$P_{sq}(s_i, q_j) = \frac{N_{sq}(i, j)}{\text{total number}}. \quad (2.4)$$

Discrete probability density functions for $X(k), X(k + \tau)$ are generated by summing the data points in each row and column of the grid respectively and dividing by the total number of attractor points.

$$P_s(s_i) = \sum_j \frac{N_{sq}(i, j)}{\text{total number}}, \quad (2.5)$$

$$P_q(q_i) = \sum_i \frac{N_{sq}(i, j)}{\text{total number}}. \quad (2.6)$$

Then calculate the mutual information based on different time delay value. Normally, it is changed from one to some finite number. When the mutual information is minimum, the attractor is as spread out as much as possible. The value of τ which gives the first minimum is the attractor reconstruction delay [18]. This condition for the choice of delay time is known as minimum mutual information criterion.

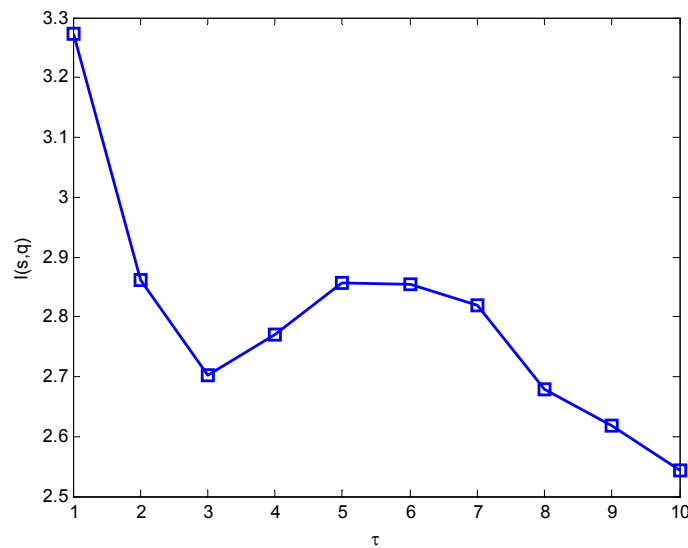


Figure 8. Mutual information value versus time delay τ .

Figure 8 shows the determination time delay for a Lorenz dynamical system using mutual information algorithm. According to minimum mutual information criterion, 3 can be seen as the optimized time delay value for this system.

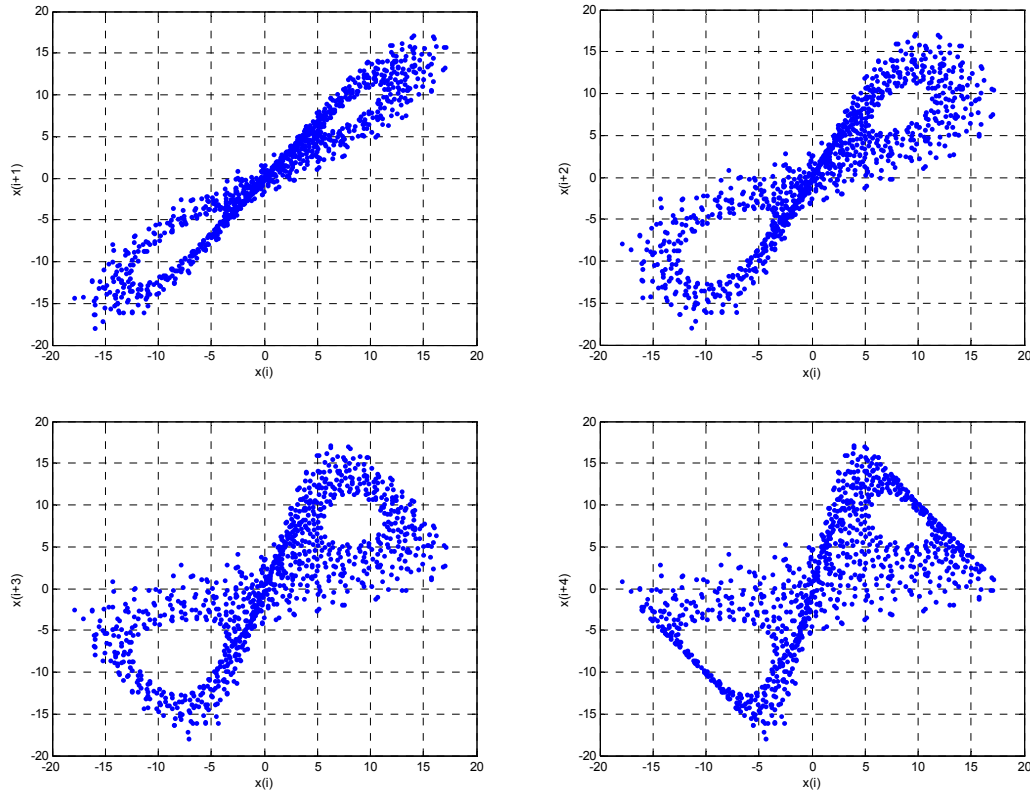


Figure 9. Reconstructed phase space for τ value 1, 2, 3, and 4.

Figure 9 shows distribution of 2D reconstructions of Lorenz attractor for different τ . As can be seen from the plots above, the attractor looks clean and opened up at $\tau = 3$ on the bottom left panel. At $\tau = 1$ or 2, the attractor is quite unrecognizable which are shown on the up two plots. This result is consistent to that from mutual information algorithm which is shown in Figure 8. Numerical results indicate that this method can determine the correct delay time. Moreover, for an infinite amount of noise free data, we are free to choose arbitrarily, the time delay.

2. Embedding Dimension

The next parameter need to be estimated after embedding lag is the embedding dimension d_e to achieve a good embedding. According to the Takens' embedding theorem [16], if d_e is sufficiently large, the evolution of $X(i)$, which is $\{x(i), x(i+\tau), x(i+2\tau), \dots, x(i+(d_e-1)\tau)\}$, will be the same as original state change. Based on this theory, as long as one picks a d_e high enough, it is fine but there are other considerations. One is that computational cost increases quickly with increasing d_e . Moreover, the conditions under this theorem are very difficult to achieve in practice. At the very least, sampled data represents a breach of the differentiability [21].

False Nearest Neighbors provides a robust way to determine necessary embedding dimensions. The basic idea of False nearest neighbor is: “two points which are close in the reconstructed state space stay close under forward iteration.” [22] That means two points close to each other should be property of the set, not of an artifact of using too low an embedding. Any property of the system that is dependent on the distance between two points will stop changing when we reach a sufficient dimension.

In d_e dimension state space, every point

$$X(i) = \{x(i), x(i+\tau), \dots, x(i+(d_e-1)\tau)\},$$

has a nearest neighbor called

$$X^{NN}(i) = \{x^{NN}(i), x^{NN}(i+\tau), \dots, x^{NN}(i+(d_e-1)\tau)\}.$$

Therefore measure the distances between this point and its nearest neighbor use a Euclidean distance:

$$R_{d_e}^2(i) = [x(i) - x^{NN}(i)]^2 + [x(i + \tau) - x^{NN}(i + \tau)]^2 + \dots + [x(i + (d_e - 1)\tau) - x^{NN}(i + (d_e - 1)\tau)]^2, \quad (2.7)$$

and the change in distance by adding one more dimension is

$$R_{d_e+1}^2(i) = R_{d_e}^2(i) + [x(i + d_e\tau) - x^{NN}(i + d_e\tau)]^2. \quad (2.8)$$

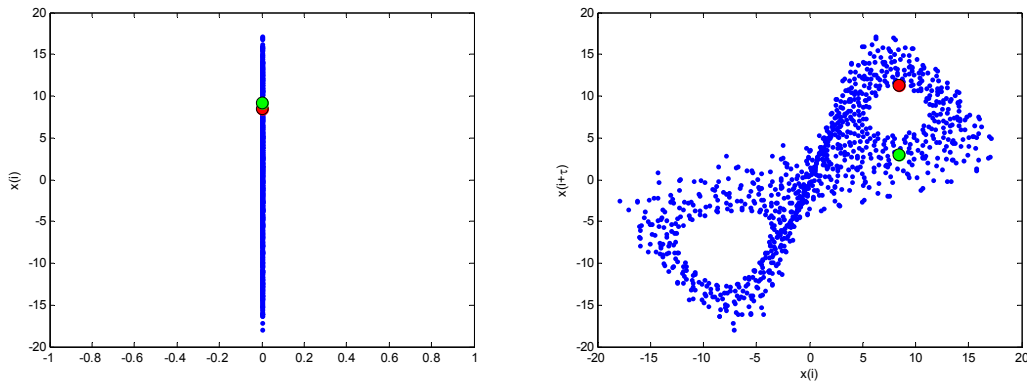


Figure 10. False nearest neighbor.

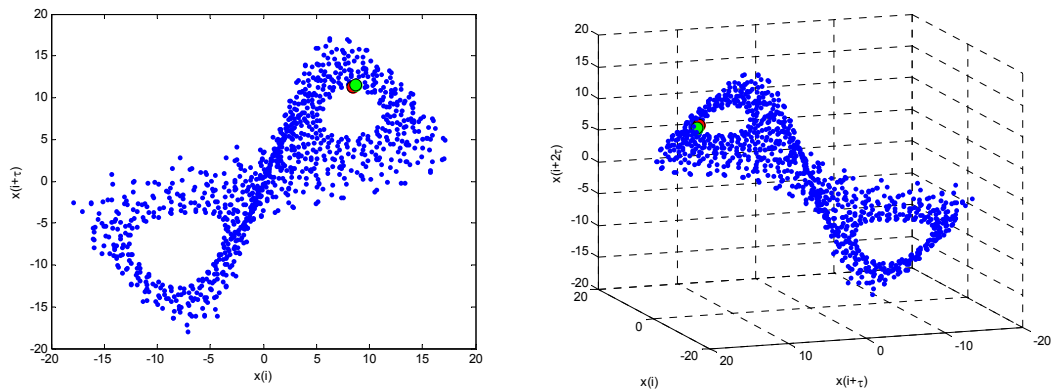


Figure 11. Real nearest neighbor.

As mentioned above, Figure 10 shows a green point and its nearest neighbor in one

dimension phase space on the left panel. The distance between them change much by adding one more dimension on the right panel. Figure 11 also shows a pair of the points that are really nearest neighbors because this value should not change too much as embedding dimension increases. The relative change in the distance can be calculated as a way to see whether these points were really close together or not [23]. Using a threshold a criterion for false nearest neighbors is shown following:

$$\frac{|x(i + d_e \tau) - x^{NN}(i + d_e \tau)|}{R_{d_e}(i)} > R_\tau. \quad (2.9)$$

In practice values of R_τ in the range $10 \leq R_\tau \leq 50$ works well for most situations. By this criterion one can then test sequence of points and, as d_e increases, find where the percentage of nearest neighbors goes to 0.

However, the false nearest neighbor algorithm is not robust to a data from a random-number generator [24]. Embedding dimension value will be too small when the criterion is applied. Additional criterion is taken into account the distances as measured with respect to the size of the attractor R_A

$$\frac{R_{d_e+1}(i)}{R_A} \geq 2. \quad (2.10)$$

A common way to estimate R_A is by using the root mean square value of the data.

$$R_A^2 = \frac{1}{N} \sum_{i=1}^N (x(i) - \frac{1}{N} \sum_{i=1}^N x(i))^2. \quad (2.11)$$

If noise is present in our signal, the higher d_e will be populated by this extra noise instead of the meaningful dynamics of the system. One can also use the false nearest

neighbors test to find the relative contamination of noise in the signal.

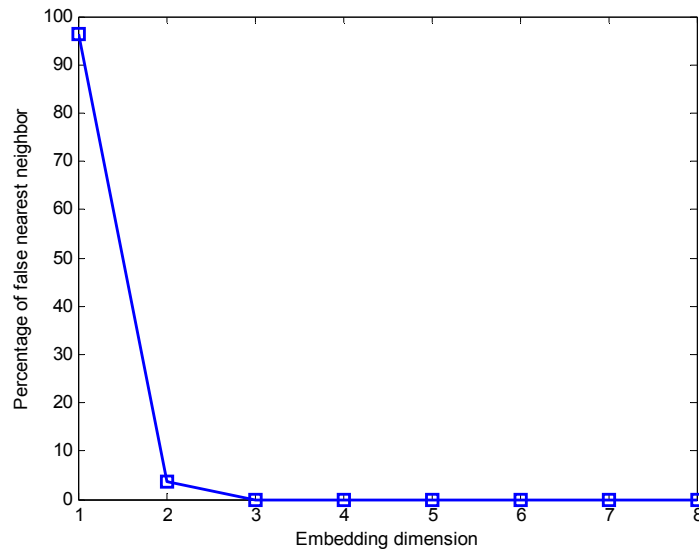


Figure 12. Percentage of false nearest neighbor for the Lorenz system.

Figure 12 shows percentage of false nearest neighbor under different embedding dimension from 1 to 8. According to the criterion mentioned previous, 3 can be seen as the suitable embedding dimension value for this system. This result is consistent to number of variables in equations (2. 1). Therefore the false nearest neigh can be assessed as an effective method to determine embedding dimension.

B. Fractal Dimension

The fractal theory is an important and active field in the nonlinear dynamic system study. Almost all chaotic systems have a quantifying measurement known as a fractal dimension which is extracted from the original or reconstructed phase space and applied

to speech recognition or classification. The state variety in a complicated mechanism could be represented by its attractor. Fractal dimension describes how an attractor takes up in phase space. Fractal dimension is a dynamic invariant does not depend on the coordinate system and different initial conditions. In other words, the value of a dynamic invariant obtained directly from the original system and they are invariant in both the original and reconstructed phase space.

In mathematics and geometry, the dimension of an object or space is defined as the minimum number of coordinates that used to specify every point in it. For example, the dimension of a line is one, the dimension of a surface is two, and a cube has a dimension of three.

The term “fractal” was coined by Benoit Mandelbort in 1975 [25] and was derived from the Latin fractus meaning "broken" or "fractured." A fractal is an object or shape that appears self-similar no matter what size it is viewed at. More clearly, each small part of a fractal object or shape will look almost the same with the structure of the whole. Fractal possesses symmetry across scale.

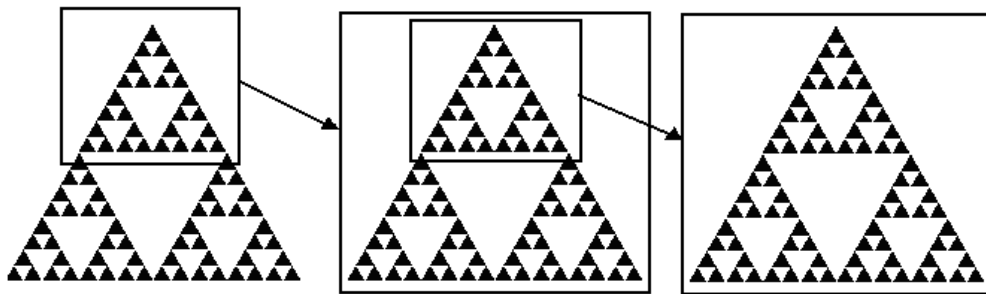


Figure 13. Sierpinski Triangle.

Sierpinski's Triangle is one of the most interesting and one of the simplest fractal shapes in existence. As shown in Figure 13, vary the magnitude of picture and zoom in on the top of these three sub-triangles, and it will look exactly the same with the entire Sierpinski Triangle itself. In fact, the previous process can be repeated as many times as possible, and each sub-triangle is an exact replica of the whole Sierpinski Triangle. It is similar to itself at different scales.

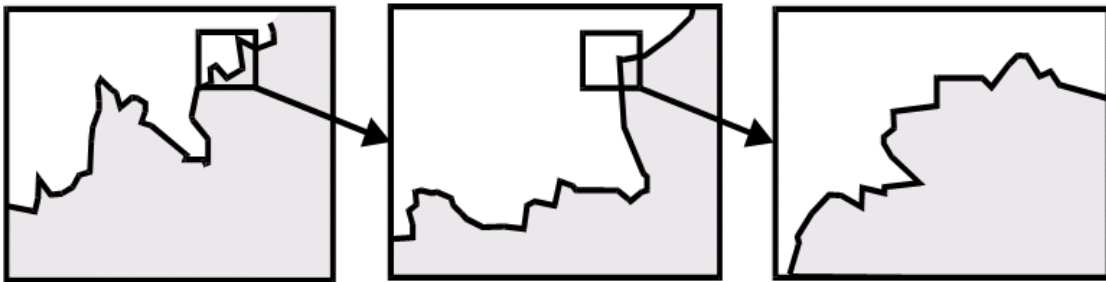


Figure 14. Segmental coast of Britain.

Fractal not only can be a mathematical or geometrical construct, but also it exists in nature. Mandelbrot began his treatise on fractal geometry by considering the question: "How long is the coast of Britain?" Figure 14 shows one segment of the coastline, the border between the land and the sea, has bays and peninsulas [26]. Ever smaller bays and peninsulas can be seen if coastline is magnified. The structure at a small scale is also similar to the structure at a large scale.

Put one map of Britain on a very large-scale. Because of irregularity of the coastline, a measure with a straight ruler, as shown in Figure 15, provides an approximation [27]. The estimated length of coastline L equals the length of the ruler R multiplied by N ,

the number of rulers used. On the left panel 1 unit length rules are chosen, $1/2$ unit length rules are used for measurement on the middle panel, while more smaller rules, $1/4$ unit length, on the right panel.



Figure 15. Measuring the length of a coastline using rulers of varying lengths.

However, the results that come from three panels using different rules are totally different. Circumference is $12 (12 \times 1)$ units on the left, $14 (28 \times 1/2)$ units in the middle, $15 (60 \times 1/4)$ units on the right side. Each time the size of rules decreases, the perimeter increases. Moreover, there is no shapes can be used to define the coastline of Britain, because exactly circumscribing the coast of Britain would entail encircling every rock, every tide pool, every pebble which happens to lie on the edge of Britain. The smaller rules there are, the closer the circumscribing line will be able to conform to the dips and the protrusions of Britain's rugged coast. In general, as the length of a ruler becomes

diminishingly small, the length of coastline will reach infinitely large. The concept of length begins to make little sense.

In fractal geometry, Mandelbrot used the fractal dimension as a statistical quantity that gives an indication of how completely a fractal appears to fill space, as one zooms down to finer and finer scales. Then one can use fractal dimension to describe the coastline of Britain instead of length. There are many specific forms of fractal dimension, such as similarity dimension, compass dimension, box-counting dimension, Hausdorff dimension, information dimension, correlation dimension, generalized Dimension. Practically, the box-counting dimension and correlation dimension are widely used, partly due to their ease of implementation.

1. Similarity Dimension

Similarity dimension directly comes from the definition of fractal dimension, it is easiest to be understood and computed. An object or shape resides in Euclidean dimension D space and its linear size is reduced by $1/r$ in each spatial direction, its measure (length for a line, area for a square, or volume for a cube) would increase to $N = r^D$ times the original. Solve for D in mathematics:


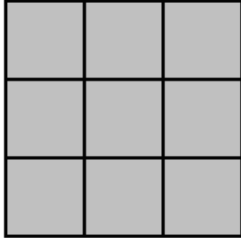
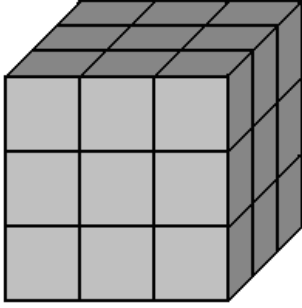
$$\begin{aligned} N &= r^D, \\ \log(N) &= D \log(r), \\ D &= \log N / \log r. \end{aligned} \tag{2. 12}$$

Similarity dimension emphasizes this common pattern and provides a way how to computing the dimension of a self-similar shape. For a self-similar object or shape, each

time it is scaled by a similarity with magnification factor r , it makes of N copies of itself, the similarity dimension is

$$D_s = \lim_{r \rightarrow 0^+} \frac{\log(\text{number of self-similar pieces, } N)}{\log(\text{magnification factor, } 1/r)}. \quad (2.13)$$

Table 1. Computed similarity dimension of objects.

A line:	A square:	A cube:
		
$r = 1/3,$ $N = 3,$ $D_s = \log(3) / \log(1/(1/3))$ $= 1$	$r = 1/3,$ $N = 9,$ $D_s = \log(9) / \log(1/(1/3))$ $= 2$	$r = 1/3,$ $N = 27,$ $D_s = \log(27) / \log(1/(1/3))$ $= 3$

As Table 1 shown above, similarity dimensions of a line, a square, and a cube are consistence with their Euclidean dimensions. This formula can be generally used to compute for the number of pieces that are scaled by similarities with different magnification factors. Examined this way, D_s need not be an integer, as it is in Euclidean geometry. It could be a fraction, as it is in fractal geometry.

Figure 16 shows the conceptual and simply way of generating the Sierpinski Triangle that mentioned in previous section. Begin with a triangle, separate it into four small triangles by connecting the midpoints of three sides, then cut out the small triangle in the center. Perform this same action for each of the three remaining sub-triangles. Iterate infinitely and final figure will be finished. Also, similarity dimension of a Sierpinski triangle can be calculated as following

$$D_s = \log 3 / \log [1 / (1/2)] = 1.5849 . \quad (2.14)$$

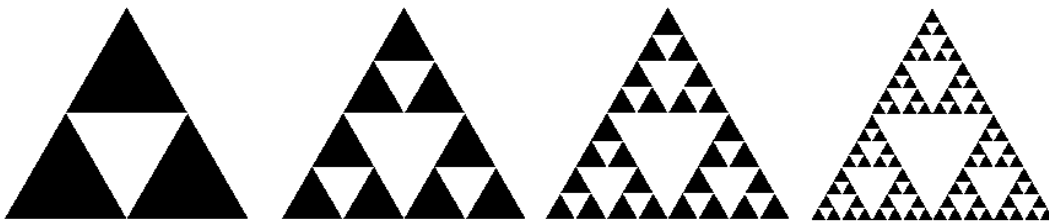


Figure 16. Geometric construction of the Sierpinski triangle.

Take Koch curve for another example, which have inspired many artists who produced amazing pieces of art. Moreover, for Benoit Mandelbrot's pioneering work on fractals, the Koch curves is one of the most important objects used by him.

The Koch curve allows numerous variations and Figure 17 introduces a fair simple way to construct it. Divide a straight line into three equal segments and replace the center segment by two segments having the same length to generate an equilateral triangle. Now each of the four resulting segments can be seen as a single straight line mentioned in the first step, process is then repeated for these 4 segments, leading to the

top right panel of Figure 17 in the second iteration of the constructional process. Iterate infinitely and final figure will be finished. Also, similarity dimension of a Koch curve can be calculated as following

$$D_s = \log 4 / \log [1 / (1/3)] = 1.2618. \quad (2.15)$$

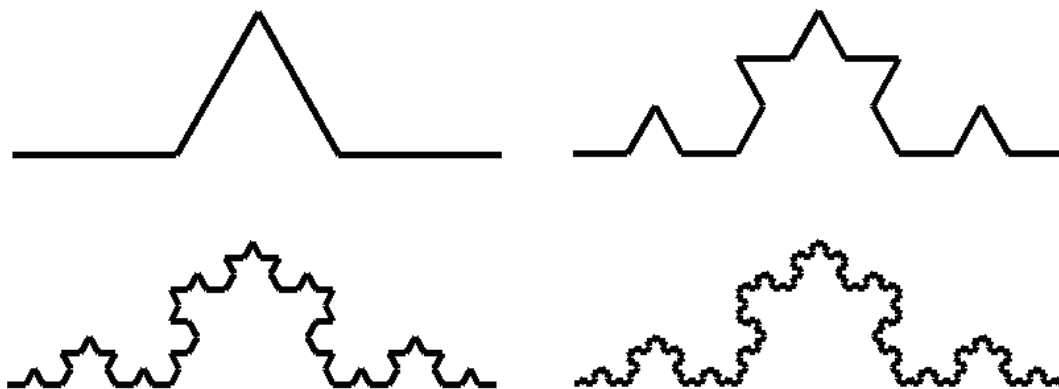


Figure 17. How the curve is recursively constructed.

Similarity dimensions are not limited to being between one and two. An object between a point and a line such as Cantor set has similarity dimension between zero and one. Further, take Menger Sponge as an example, a similarity dimension of between two and three would represent an object which occupies more space than a plane, but less than a sphere.

2. Box-Counting Dimension

Besides similarity dimension, the box-counting dimension “ D_b ” is also one kind of

fractal dimensions. Generally none real-world object or shape has clearly repeating self-similar structure as Sierpinski triangle and Koch curve. It means that the similarity dimension algorithm will not work because real-world objects have less regular shapes and cannot be divided into equal segments. Therefore, there will be a problem when measuring the fractal dimension of real-world shape as a coastline or part of it which mentioned at the beginning of this chapter. In such cases box-counting dimension is more widely used, which is often based on calculating occupied boxes algorithm [28].

The algorithm of box counting dimensions assumes a set S contained in n dimension Euclidean space. For any $r > 0$, divide this n dimension Euclidean space into a very fine grid with n -dimensional cubes of side-length r , and $N_r(S)$ be the minimum number of small cubes needed to cover S . If there is a number D_b so that

$$N_r(S) \sim 1/r^{D_b} \text{ as } r \rightarrow 0. \quad (2.16)$$

The number D_b is defined as the box-counting dimension if and only if there is some positive constant k so that

$$\lim_{r \rightarrow 0} \frac{N_r(S)}{1/r^{D_b}} = k. \quad (2.17)$$

Solving for D_b gives

$$\begin{aligned} \lim_{r \rightarrow 0} (\log N_r(S) + D_b \log r) &= \log k, \\ D_b &= \lim_{r \rightarrow 0} \frac{\log k - \log N_r(S)}{\log r} = \lim_{r \rightarrow 0} \frac{\log N_r(S)}{\log(1/r)}. \end{aligned} \quad (2.18)$$

Note that the $\log(k)$ term drops out when r becomes infinitely small. Moreover, n -dimensional small cubes are not necessary if some other shape is more convenient.

Disks of diameter, or even stars of diameter can be used to cover set S instead of cubes and the answer D_b will not change [29].

However, the data used for computer calculation is discrete time series rather than continuous. That means the sampling interval of r is unable to approach infinitely small even the data is sampled at very high rate. In the actual calculation it will use an approximate algorithm which works very well for any object or shape provided as a monochrome image.

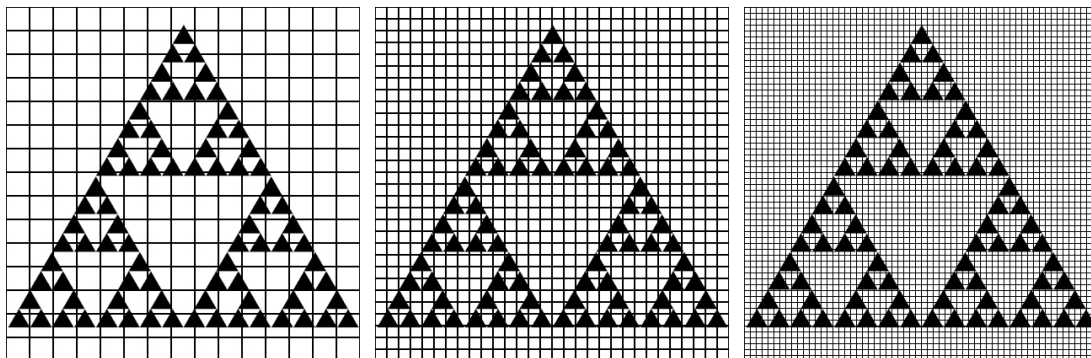


Figure 18. Covering the Sierpinski triangle with smaller and smaller boxes.

As shown in Figure 18 left panel, a grid is put over the Sierpinski triangle image. Then calculate the number of boxes which contain part Sierpinski triangle. At the next step shown on center panel in Figure 18 a lower grid is chosen and again those boxes, which contain a relevant part of the image, are calculated. Then repeat. That means be different from similarity dimension by dividing image into segments, box-counting method just change the grid.

Table 2. Calculate the occupied boxes of each grid-size.

Box Size	Count No.		
r	Nr	$\log_2(1/r)$	$\log_2(Nr)$
21x21	470	-4.3923	8.8765
27x27	304	-4.7549	8.2479
29x29	271	-4.858	8.0821
35x35	196	-5.1293	7.6147
41x41	153	-5.3576	7.2574
51x51	113	-5.6724	6.8202
61x61	88	-5.9307	6.4594
65x65	78	-6.0224	6.2854
73x73	65	-6.1898	6.0224
87x87	48	-6.4429	5.585
101x101	36	-6.6582	5.1699

When computing box dimension, some simplifications can be made [29]. To make the calculations much easier, not every possible r need to be considered. Choosing a convenient sequence where r_i is a sequence converging to zero is enough to consider the limit of $\log N_r / \log r$. Table 2 shows some r that be chosen. Calculate the occupied boxes of each grid-size.

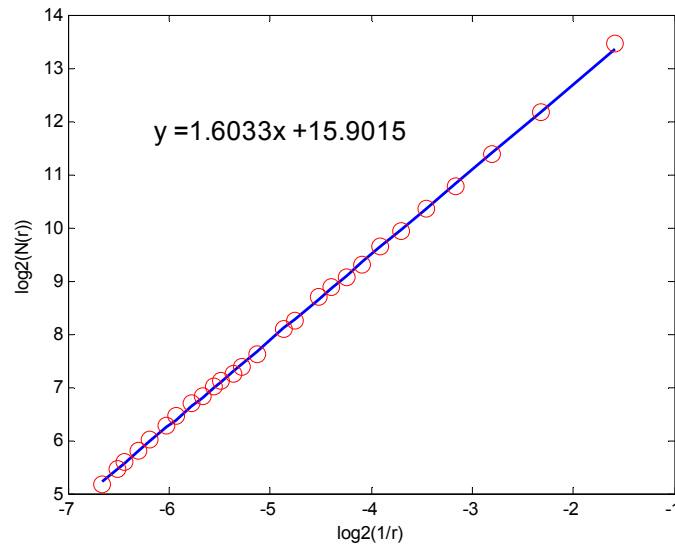


Figure 19. Log-Log plot to estimate the box-counting dimension.

The number of boxes N_r and the grid width r can produce a dual logarithm curve that should fulfill the following linear regression model [12]

$$\log_2(N_r) = D_b \cdot \log_2(1/r) + b. \quad (2.19)$$

Figure 19 plots the points in the Table 2 (the graph shows a greater range, and more widely spaced, points than table), then the least square method is applied to obtain the slope of the straight line and the box counting dimension is the value of slope. So the box-counting dimension of the Sierpinski triangle is about 1.60.

Then this procedure is used for Koch Curve which mentioned in previous section. The points are plotted that lie on a straight line of slope about 1.29 in Figure 20. So the box-counting dimension of the Koch curve is about 1.29.

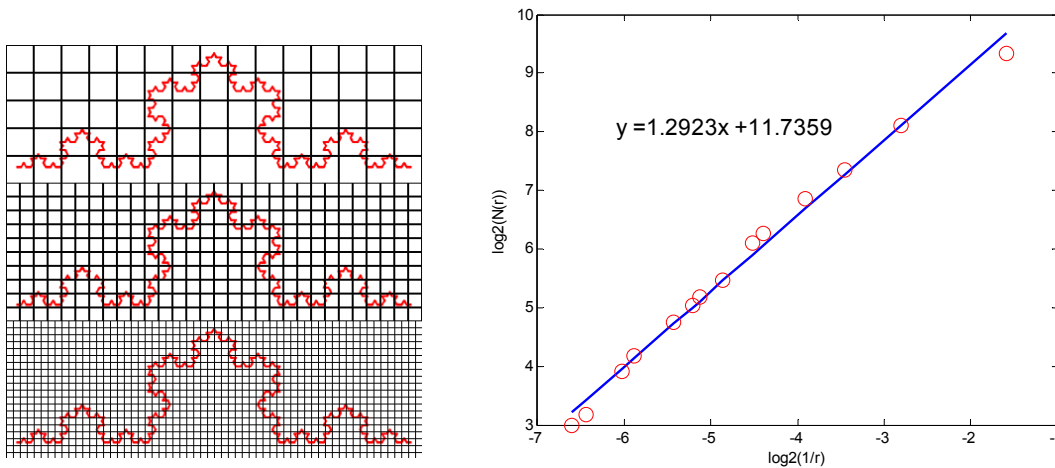


Figure 20. Box-counting dimension estimation of the Koch Curve.

From the results above and previous chapter, the box-counting dimension of Sierpinski triangle is 1.6033, and from the fractal definition its similarity dimension is 1.5849; the box-counting dimension of Koch curve is 1.2923, and from the fractal definition its similarity dimension is 1.2618; These errors, 1.16% and 2.42% respectively, are acceptable, Therefore, it is concluded that the box-counting dimension can provide an effective method to calculate fractal dimension.

One must use the same dimension ruler to measure the same dimension quantity. For example, use a ruler to measure a line. If one measures a square by using a line or a point, the answer will be infinite. Go back to the question "How long is the coast of Britain?" As shown in Figure 21, the box-counting dimension of coastline of Britain is 1.39. That means exactly right answer can be got if and only if the coastline is measured by using a 1.39 dimension "ruler".

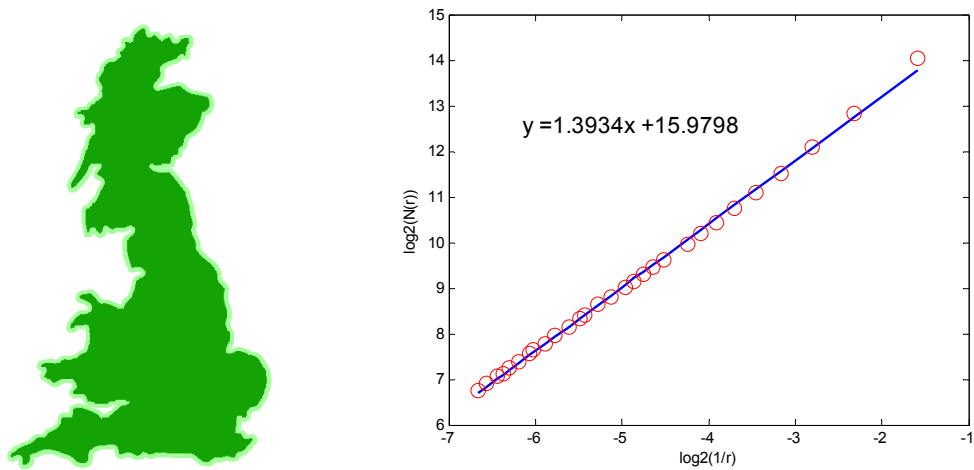


Figure 21. Box-counting dimension of coastline of Britain.

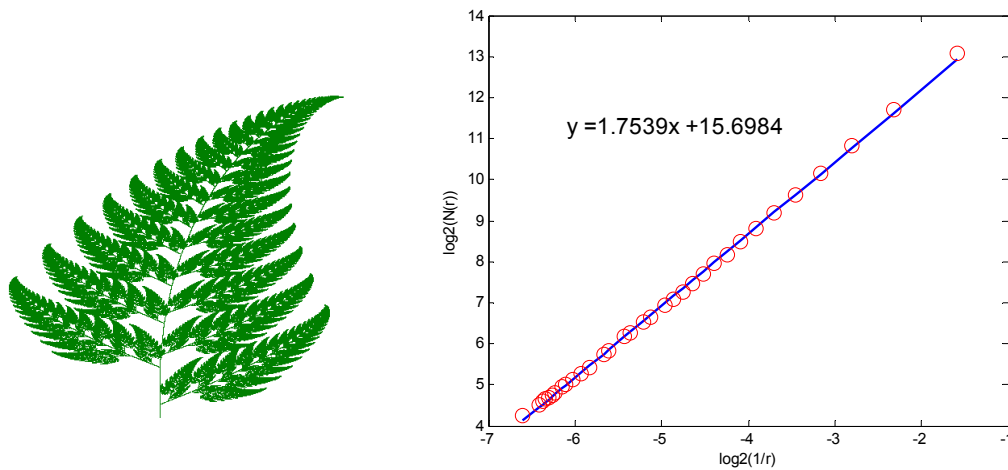


Figure 22. Box-counting dimension of Barnsley Fern.

The Barnsley Fern is a fractal named after the American mathematician Michael Barnsley who first described it in his book *Fractals Everywhere*. Like the Sierpinski triangle, the Barnsley fern shows how graphically beautiful structures can be built from

repetitive uses of mathematical formulas with computers in Figure 22. The Box-counting dimension of a Barnsley Fern is 1.75.

3. Correlation Dimension

Similarity dimension and box-counting dimension are simpler and more easily understood than the others. Such as those described in the previous sections, similarity dimension is very suitable to calculate for fractals generated from simple iterative rules while box-counting dimension is useful for monochrome images. However, the phase spaces are usually high dimension Euclidean space. When dimension goes higher and higher, the algorithmic complexity grows exponentially with the set dimension [30], calculating box counting dimension require a prohibitive amount of computation time. Thus, the box-counting dimension can be computed only for low-dimensional sets. Correlation dimension is a good substitute for the box-counting dimension due to its computational simplicity. It is successfully used to estimate the dimension of attractors of dynamical systems.

Being one of the characteristic invariants of nonlinear system dynamics, the correlation dimension can measure the complexity for the attractor of the system in phase space, it is given by

$$D_c = \lim_{r \rightarrow 0} \frac{\sum_{i=1}^{M(r)} P_i^2}{\log r}. \quad (2.20)$$

Like algorithm of box-counting dimension, divide n dimension Euclidean phase space into a very fine grid with n -dimensional cubes of side-length r . P_i is the

probability to find a point of the attractor in the i^{th} sub-cube of phase space. $M(r)$ is the total number of sub-cubes that contain attractor points

$$M(r) \sim \left(\frac{1}{r}\right)^{D_c}. \quad (2.21)$$

After time delay and embedding dimension are decided, the attractor of the dynamic system can be reconstructed. Then the Grassberger and Procaccia (G-P) algorithm which allows an accurate and efficient numerical computation of the attractor's dimension can be directly applied to the reconstructed phase space to calculate the correlation dimension.

The correlation dimension is closely related to the correlation integral $C_{de}(r)$ which is defined in the d_e -dimensional reconstructed space as the probability of finding a pair of vectors whose distance is not larger than r . It is given by Grassberger and Procaccia as follows :

$$C_{de}(r) = \lim_{n \rightarrow \infty} \frac{1}{n^2} \times [\text{number of pairs of } i, j \text{ whose distance } |X_i - X_j| < r], \quad (2.22)$$

where

$$X_i = \{x(i), x(i + \tau), x(i + 2\tau), \dots, x(i + (d_e - 1)\tau)\}.$$

More formally correlation dimension is defined using Heaviside function:

$$C_{de}(r) = \frac{2}{N(N-1)} \sum_{i=1}^N \sum_{j=i+1}^N H(r - r_{i,j}), \quad (2.23)$$

where $H(x)$ is the Heaviside Step function:

$$H(x) = \begin{cases} 1, & x \leq 1 \\ 0, & x > 1 \end{cases}, \quad (2.24)$$

r is the distance parameter, r_{ij} is the distance between two vectors in reconstructed phase space, which is computed using the Euclidean norm

$$r_{ij} = \|X_i - X_j\| = \left[\sum_{m=0}^{de-1} (x(i+m\tau) - x(j+m\tau))^2 \right]^{1/2}. \quad (2.25)$$

The correlation dimension D_c based on G-P algorithm is defined as

$$D_c(d_e) = \lim_{r \rightarrow 0} \frac{d \log_2 C_{de}(r)}{d \log_2 r}. \quad (2.26)$$

To be the same with the algorithm of box-counting dimension, the value of r is unable to approach infinitely small because of discrete time series. In practice, one usually locates a linear scaling region from the plot of $\log_2(C_{de}(r))$ versus $\log_2(r)$, and estimates the slope of the curve over the linear region. This slope is an estimation of the correlation dimension $D_c(d_e)$ of the original attractor in the d_e -dimensional reconstructed phase space.

As shown in Figure 23, the correlation integral of Lorenz system is plotted logarithmically against $\log_2(r)$ on the up panel. The slope of line is plotted as a function of $\log_2(r)$ on the bottom panel. When it reaches a plateau for a range of large enough values, then the value (about 2.06 in this case) is taken to be an estimation of the true correlation dimension D_c for the system.

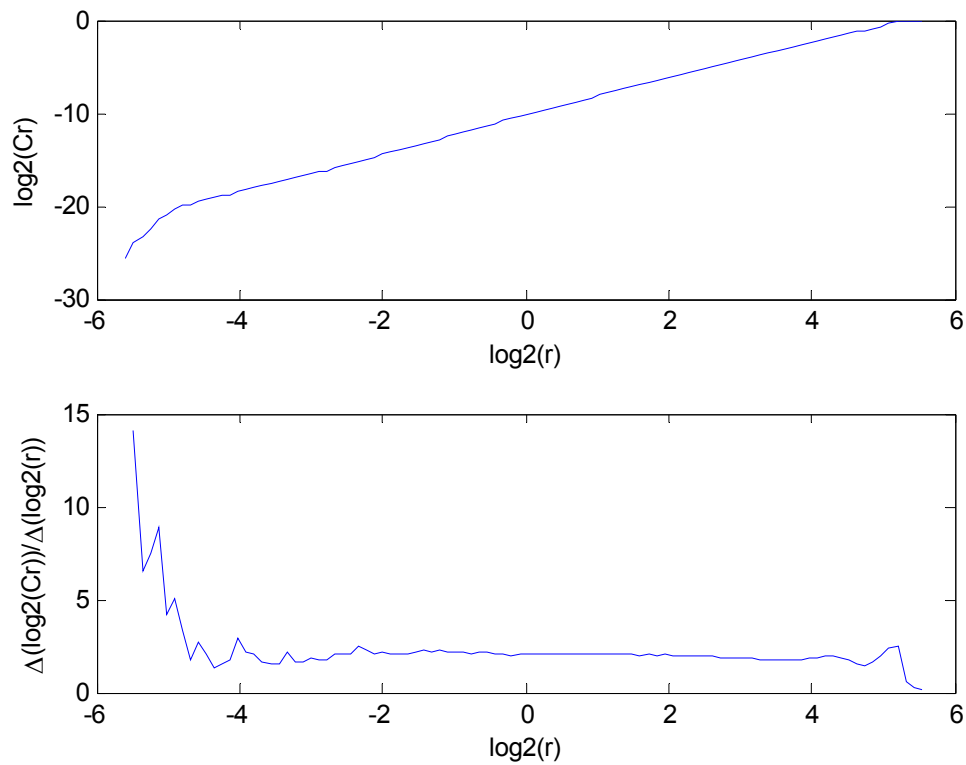


Figure 23. Correlation dimension of Lorenz system.

As shown in Figure 24, the correlation integral of Rossler system is plotted logarithmically against $\log_2(r)$ on the up panel. The slope of line is plotted as a function of $\log_2(r)$ on the bottom panel. When it reaches a plateau for a range of large enough values, then the value (about 1.90 in this case) is taken to be an estimation of the true correlation dimension D_c for the system.

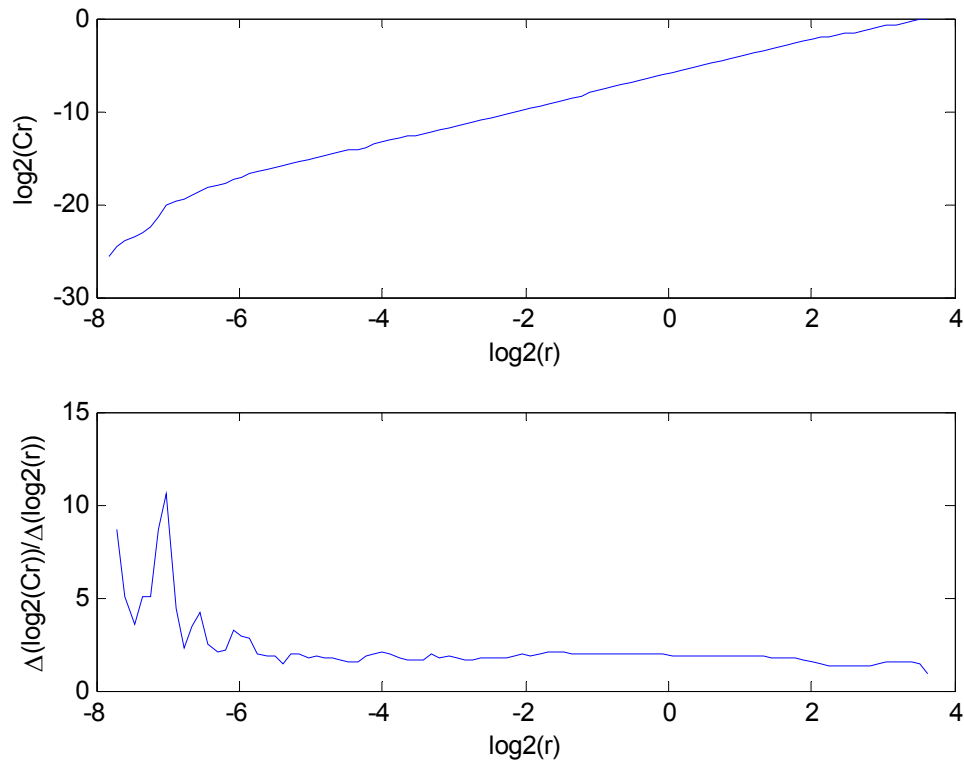


Figure 24. Correlation dimension of Rossler system.

4. Influencing Factors on the Correlation Dimension

Not only the embedding dimension and the lag time but also the data length and the noise level are important factor that influences the computational precision significantly [31].

The computational results of correlation dimension for the Lorenz and Rossler attractors are listed in Table 3 in detail. Comparison of the values for the two models with different data lengths, the expected value is 2.02 and 1.89 respectively [32], [33]. One can see that when data length larger than 4096, the related error for the Lorenz

attractor is less than 2%. While for small size data, when $N = 2048$, the related error is higher than 6%. Generally, for the data sampled at same rate, the computational precision increases as the data size increases, large data sets tend to produce a better estimation of correlation dimension than small data sets.

Table 3. Computational results of correlation dimensions with different sample size.

Attractor		Data Length			
		1024	2048	4096	8192
Lorenz (2.02)	Result	2.224	2.152	2.042	2.014
	Error (%)	10.095	6.510	1.073	-0.278
Rossler (1.89)	Result	1.870	1.712	1.924	1.859
	Error(%)	-1.079	-9.434	1.784	-1.635

In practical application the measured time series are inevitably contain noise. A low correlation dimension indicates a deterministic system. A high correlation dimension is indicative of randomness. Noise or random system fills its phase space uniformly and the correlation dimension is proportional to the embedding dimension [13].

Figure 25 shows the correlation integrals and the correlation dimension of a Lorenz and Rossler systems signal imposed with different levels of white noise. If the noise level is low, $SNR > 55$ (defined as energy ratio of signal to noise), the relative error is smaller than 10%. The numerical results indicate that the presence of noise leads to an increase of the correlation dimension. Therefore, it is necessary to preprocess the data

using noise reduction methods if non-linear time series analysis is used to analyze experimental or practical signals.

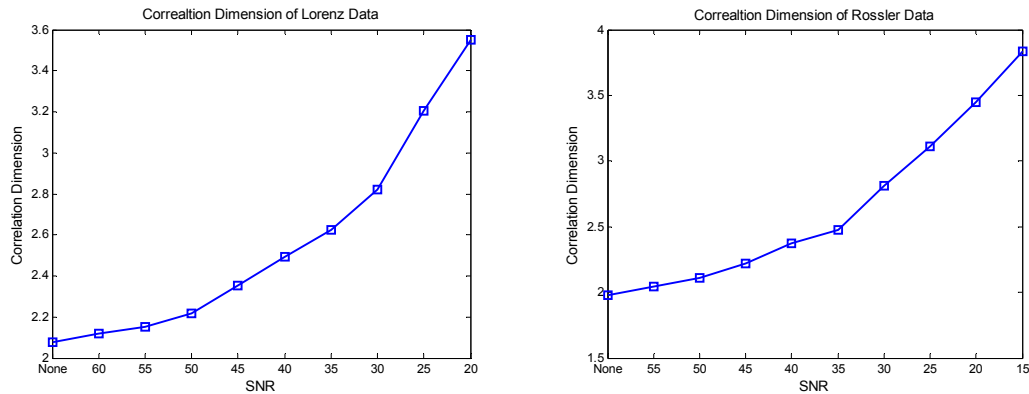


Figure 25. Correlation dimension imposed with different levels of white noise.

C. Summary of Faulty Detection Algorithm

Before collected data being applied in fault detection algorithm directly, some digital signal processing need to be finished firstly. For vibration signal, because presence of noise leads to an increase of the correlation dimension, threshold de-noising method is used for filtering background noise. For electric signal, to reduce computational time, resample the signal from 8kHz to 1.92kHz. Based on the assumption that components at integer harmonic frequencies do not contain fault information, filters are used for filtering harmonic frequencies. This procedure can make change of correlation dimension significant. Only current signal is used for phase space reconstruction and fractal dimension analysis.

The basic processes of the fractal analysis model and its procedures for estimating

and forecasting health condition of the induction motors are explained in Figure 26.

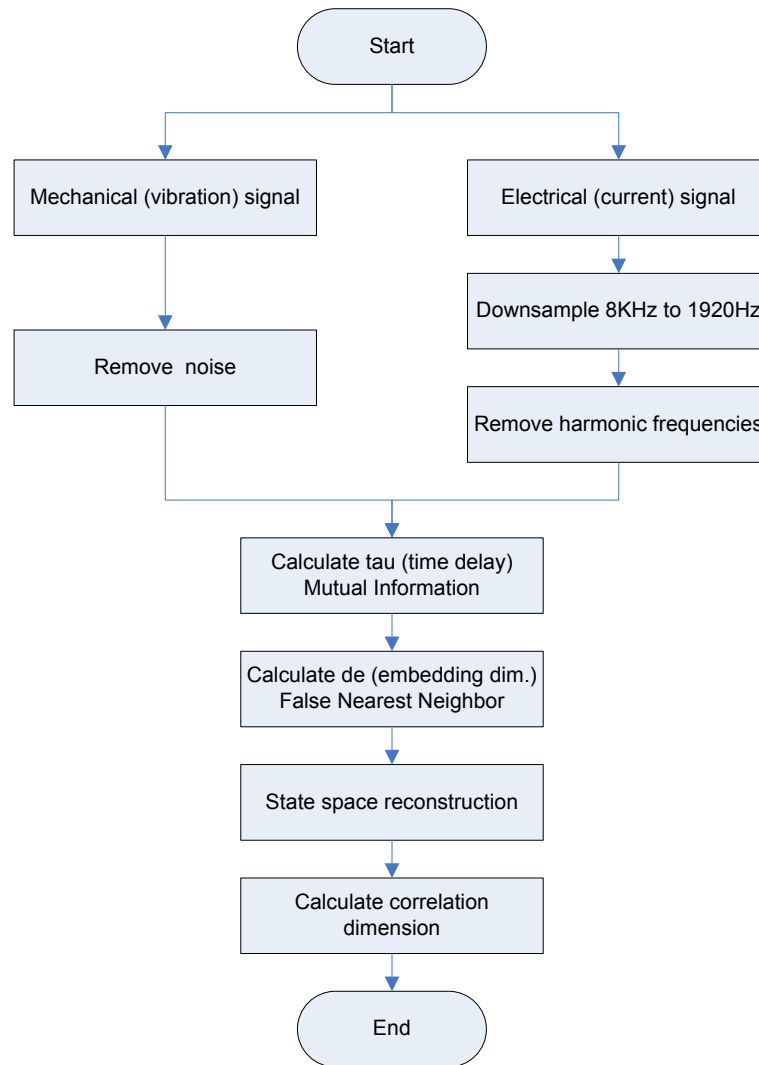


Figure 26. Summary of faulty detection algorithm.

CHAPTER III

EXPERIMENTAL SETUPS FOR IN-SITU BEARING DAMAGE

A. In-situ Bearing Fault

One of the reasons for a bearing damage and eventually a bearing failure is bearing currents. Modern AC Converters have a high du/dt combined with a high switching frequency. This results in the sum of the 3 phase voltages not being zero anymore. This nonzero and high-frequency common-mode voltage can be considered to be the root cause for different kinds of bearing currents. Basically the damage is always caused by partial discharge. The so called Electrical Discharge Machining (EDM). This film of lubricant serves as a dielectric and allows the bearing to behave as a capacitor. Figure 27 shows the created capacitor within a bearing between inner /outer race and the ball. This capacitor will be charged by the bearing currents. As soon as the voltage level is high enough it will be discharged by short circuit. Such periodically discharging will lead to an eroding of the metal.

In order to develop a bearing fault detection method, bearing fault data must be acquired before being applied in prognosis. Such data can be created off-line. That is, to disassemble the bearing, damage it, and then assemble the machine in order to collect fault data. It has been demonstrated in [14] the act of this process significantly alters the current and vibration characteristics of the machine and corrupts the experimental data. It is invalid for use in bearing condition monitoring scheme. Therefore, there is a necessary to facilitate an online, in situ failure process to conduct bearing failure

research.

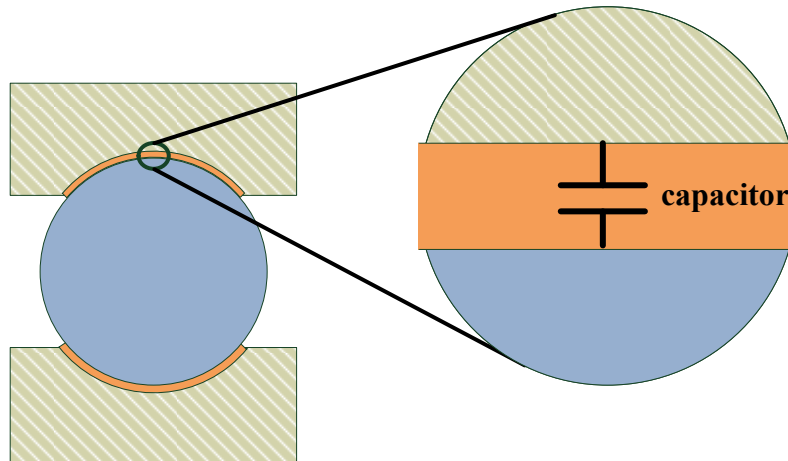


Figure 27. Created capacitor within a bearing.

The experimental method employed in the previous research where the data came from utilized a shaft current to generate online, in situ bearing faults. EDM currents flow from the shaft through the bearings to the frame and finally to the grounding point. A healthy bearing possesses a film of lubrication ranging from 0.2 to 2.0 μm thick at normal operating speeds. Given this thickness of lubrication, EDM currents can be caused by 60-Hz shaft voltages as low as 0.2–2 V peak. The current path is illustrated with the dashed line in Figure 28. Shaft current bearing damage experiments are conducted to induce and progress a bearing fault in an accelerated timeframe. These faults were generated in situ without disrupting the operation of the electric machine. This also contributes to the authenticity of the test data.

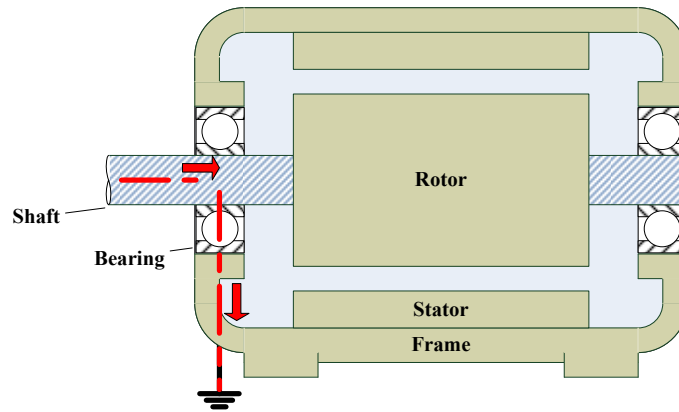


Figure 28. Use a shaft current to generate online, in situ bearing faults.

B. Shaft Current Experimental Setup

In research, two test beds were used for experimental purposes. In the first test bed, 1HP, 3 Phase, 208V induction motor G563 from Marathon Electric Company was loaded by a blower. In the second test bed, 7.5HP, 3 Phase, 208V induction motor 3KX07G manufactured by DAYTON was tested. A synchronous generator was used to load the induction motor.

Figure 29 shows a photograph a schematic diagram of these test beds. The motor used for test is powered by a three phases, 208V AC power. In this setup, an external voltage source is applied to the shaft of the motor via a carbon brush. Because of convenience and availability, a single-phase, 120V 60Hz AC power is used for providing the shaft voltage. This causes a current to flow from the shaft through the bearing. An aluminum disk is mounted on the shaft to provide a smooth contact surface for the brush. Therefore, the high bearing damage current does not affect the proper operation of the power supply.

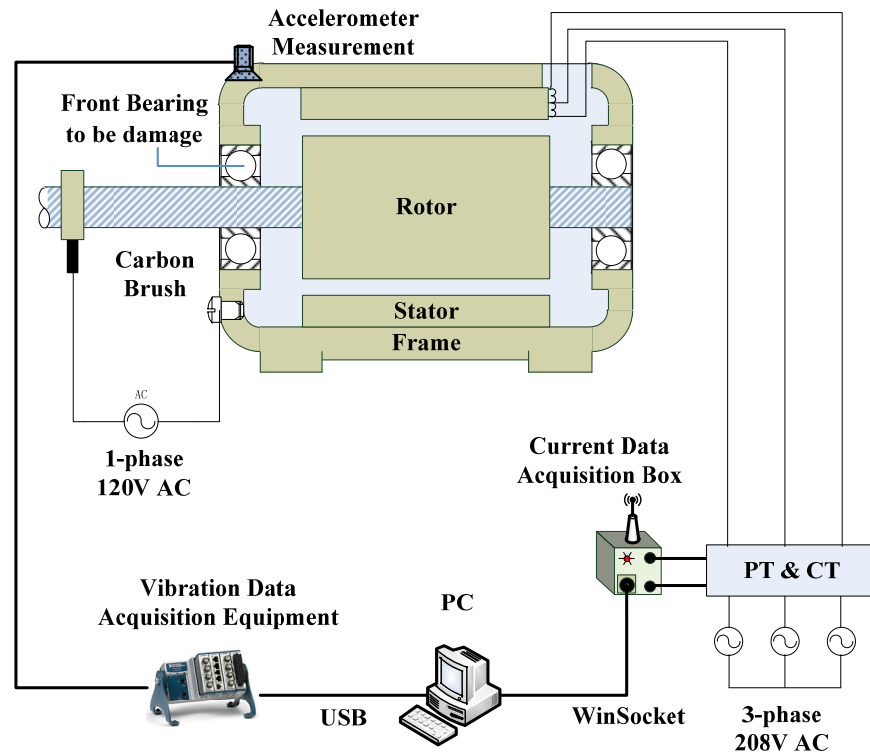


Figure 29. Experimental setup of the motor test-bed.

In vibration data acquisition system, an accelerometer 352C33 is used as motor vibration sensor, which is mounted on the top of the induction motor bearing that is damaged during the experiment. This accelerometer is capable of measuring $-50G$ to $+50G$ with the sensitivity of $100mV/G$ from $0.2Hz$ up to $5000Hz$. NI USB-9234 is ideal for a wide variety of mobile/portable applications such as industrial machine condition monitoring and in-vehicle noise, vibration, and harshness testing. It is a USB-based four-channel C Series dynamic signal acquisition module for making high-accuracy audio frequency measurements from sensors. The NI cDAQ-9174 is a four-slot NI Compact DAQ chassis designed for small, portable, mixed-measurement test systems.

Combine the cDAQ-9174 with up to USB-9234 module for a custom digital I/O measurement system which is shown in Figure 30. A Virtual Instrument (VI) program that runs under the NI LabView on PC saves the experimental measurements into data files.

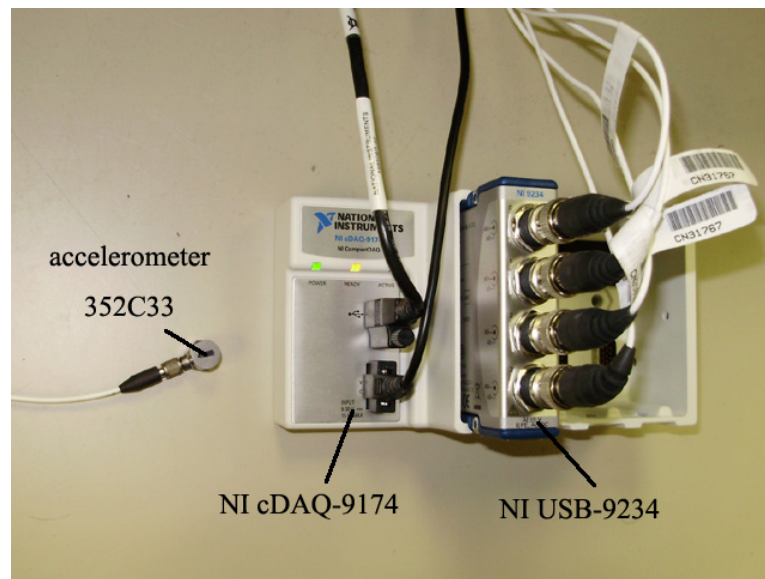


Figure 30. Vibration signal data acquisition system.

In electric data acquisition system which is shown in Figure 31, the motor line voltages and phase currents are measured by using potential transducers (PT) and current transducers (CT), respectively. The AD73360 is a six-input channel analog front-end processor. It is particularly suitable for industrial power metering as each channel samples synchronously. With this one can sample 3 channels voltage signals and 3 channels current signals. Sampling rate is set at 8 kHz. A serial port (SPORT) allows easy interfacing of single or cascaded devices to industry standard DSP engines. The

endpoint software is built around the Analog Devices VDK kernel. This is a multi-threaded kernel that provides the necessary support for the Ethernet interface. This support comes in the form of driver software and a TCP/IP stack. The data transfer algorithm is based on winsocket programming.

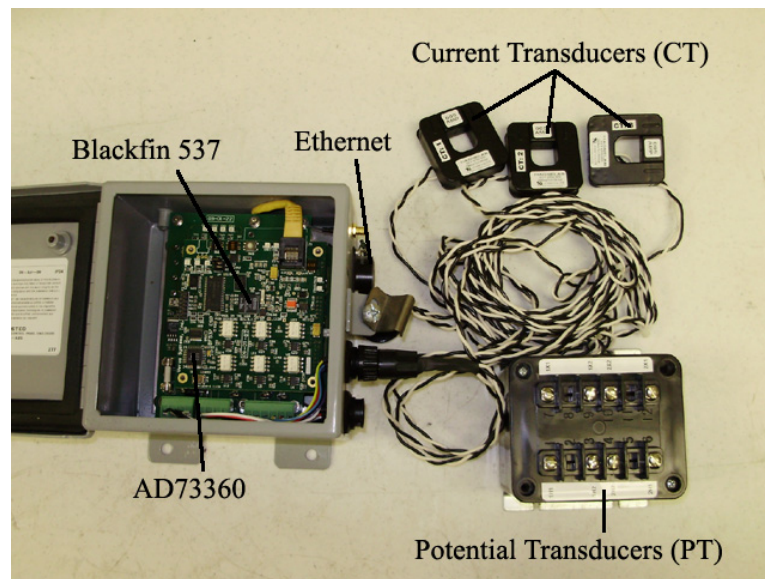


Figure 31. Electric signal data acquisition system.

Figure 32 shows an example of socket APIs used for iterative server design. The socket API specifies a socket descriptor that creates an endpoint. After the socket descriptor is created, a bind function gets a unique name for the socket. The listen function allows the server to accept incoming client connections. The server uses the accept function to accept an incoming connection request. The accept call will block indefinitely waiting for the incoming connection to arrive from an IPv4 or IPv6 client. PC uses the connect function to establish a connection to the server. The send function

sends the data request to the server. The `recv` function receives data from the server application. The `close` function closes any open socket descriptors.

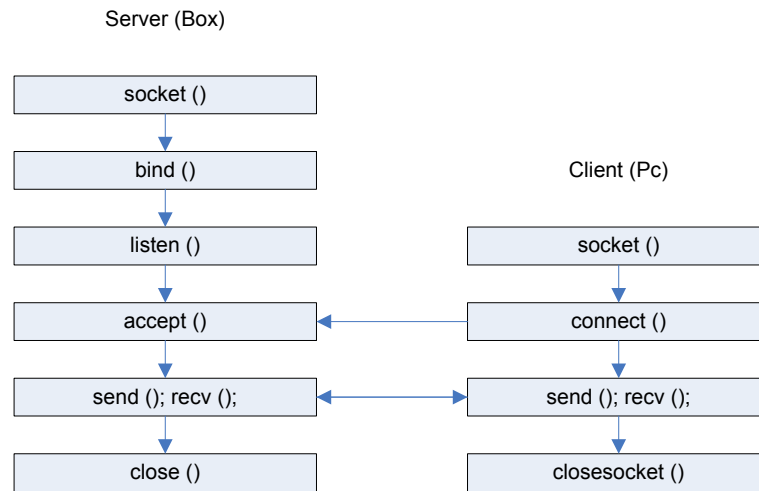


Figure 32. An example of socket APIs used for iterative server design.

CHAPTER IV

EXPERIMENTAL RESULTS

The results based on fractal analysis of two previous experimental are presented in this chapter. The set of data com from each experiment is grouped into two parts. The first part of data mechanical (vibration) signal; the second part of data is electrical (voltage/current) signal. At last, to justify the extended application of detecting other fault rather than bearing, the algorithm is also applied to a set of practical data. Though only current signal is used for phase space reconstruction and fractal dimension analysis, voltage signal can be applied to check power quality. Therefore the power input can be kept the same during experiment to eliminate correlation dimension rising caused by voltage change.

A. Induction Motor G563 Loaded by a Blower

In this experiment which is shown in Figure 33, a 1HP, 3 Phase, 208V small induction motor G563 from Marathon Electric Company was used for test. It was loaded by a “healthy” blower. To testify the algorithm mentioned in Chapter III, both health and fault signal data are needed. Firstly, the test-bed was run for about 1 day to collect healthy vibration and electric data. Then inject the shaft current, around 5 to 10 A, for around 12 hours so that the bearing is damaged. This procedure is to generate roughness bearing fault so that the performance of load side bearing deviate from the healthy range. Last, remove the shaft current and collect 1 day fault data.

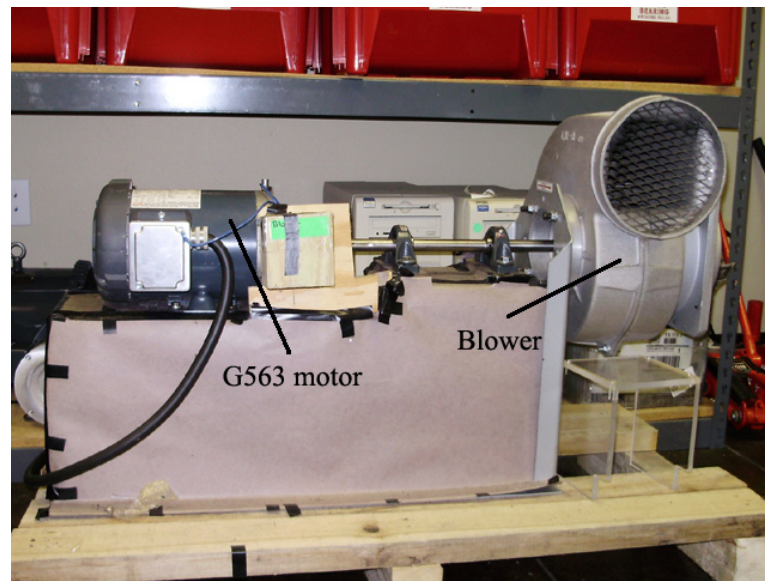


Figure 33. Experimental setup for G563 induction motor loaded by a blower.

1. Vibration Signal Analysis

The sampling rate of vibration signal is set at 12.8 kHz. Each data file is recorded by LabView on PC every minute. It contains one minute length signal. Before data being applied in fault detection, threshold de-noising method based on wavelet is used for filtering background noise. The detail setting for de-noising is shown as follows. Select the db30 wavelet, level 8, entropy type sure, and threshold parameter 1.0 based on soft threshold algorithm. However, it is very time consuming if all the sampled data is used for correlation dimension calculation. Thus, 10K points (about 9 seconds) data is applied to the algorithm to represent whole minute.

To reconstruct the phase space, two important parameters, time delay and embedding dimension need to be determined. Referring to Figure 34, a time lag of 4 is appropriate and an embedding dimension of 12 is sufficient.

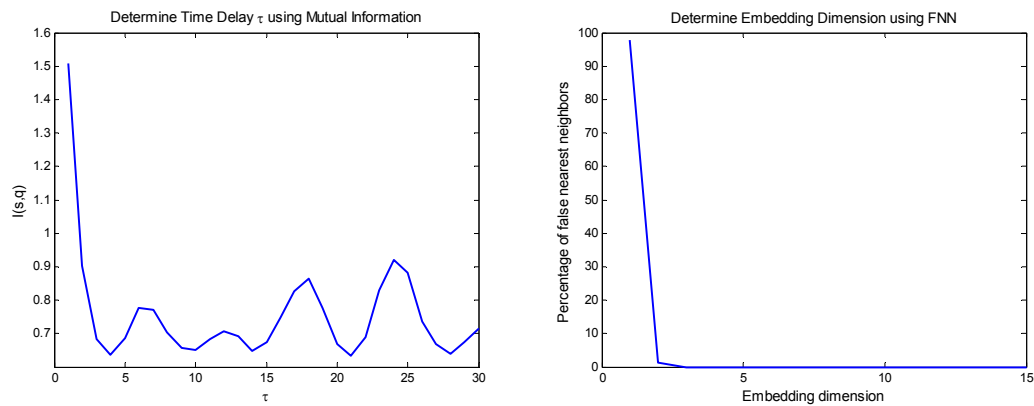


Figure 34. Average mutual information and embedding dimension.

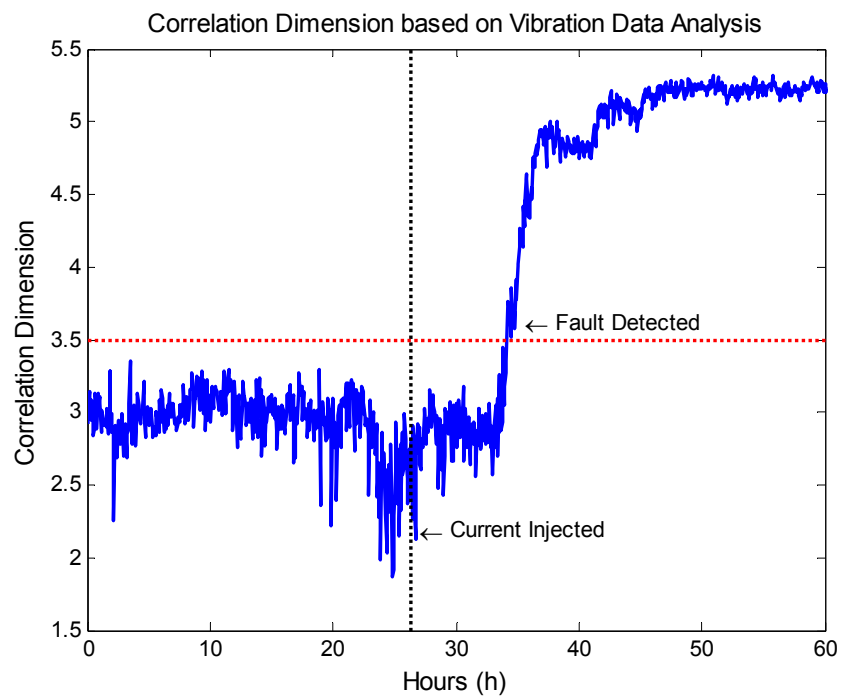


Figure 35. Correlation dimension based on vibration data analysis.

The result of first experiment based on vibration signal analysis is shown in Figure 35. In this experiment, the values of correlation dimension never go higher than 3.5 in

first 26 hours where the bearing of motor can be seen as health. The shaft current is injected at about 26th hour after the experiment started. The correlation dimension is rising because the bearing is damaged. The value of threshold is set at 3.5. The bearing fault can be detected at 36th hour. In the last 20 hours where the motor bearing is in fault state, the correlation dimension goes around 5.1. And the related deviation is 60%.

2. Current Signal Analysis

The sampling rate of electric signal is set at 8 kHz. It is sampled by AD converter and then transferred by BF537 to PC every 30 seconds. To reduce computational time, resample the signal from 8kHz to 19.2kHz and just use one data file set to the algorithm to represent ten minutes. Moreover, before current data is applied in fault detection, filter bank based on wavelet is used for filtering harmonic frequencies.

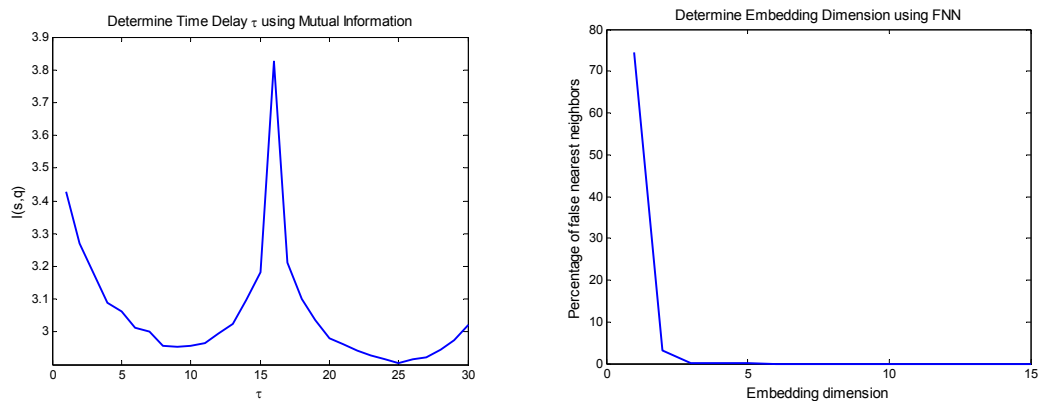


Figure 36. Average mutual information and embedding dimension.

To reconstruct the phase space, two important parameters, time delay and

embedding dimension need to be determined. Referring to Figure 36, a time lag of 8 is appropriate and an embedding dimension of 12 is sufficient.

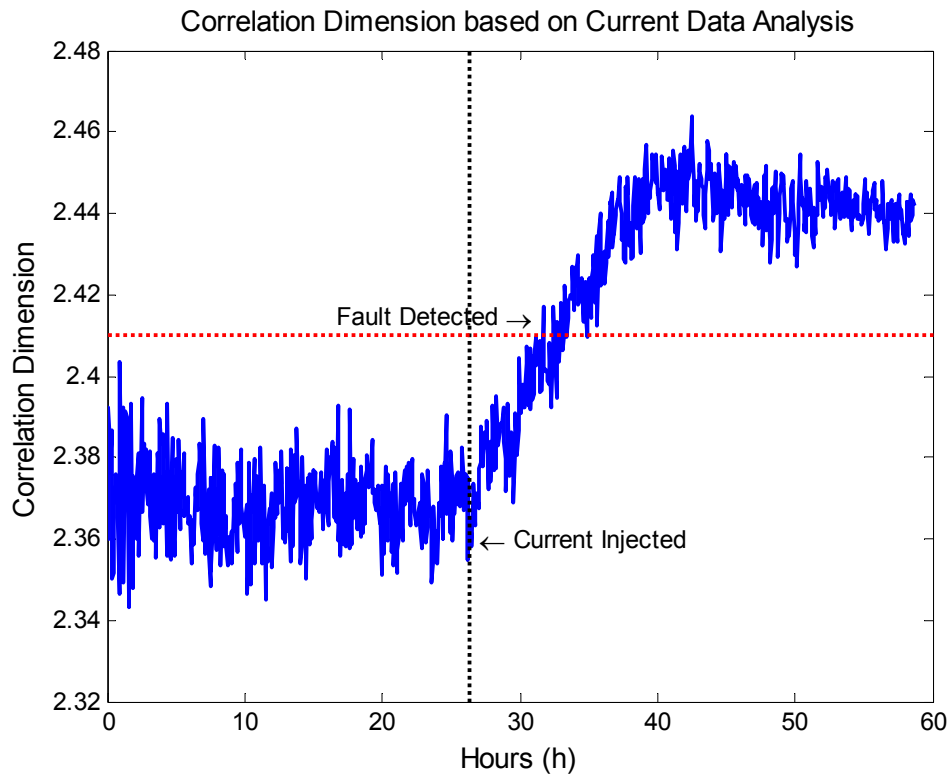


Figure 37. Correlation dimension based on current data analysis.

The result of first experiment based on current signal analysis is shown in Figure 37. In this experiment, the values of correlation dimension never go higher than 2.41 in first 26 hours where the bearing of motor can be seen as health. The shaft current is injected at about 26th hour after the experiment started. The correlation dimension is rising because the bearing is damaged. The value of threshold is set at 2.41. The bearing fault can be detected at 33th hour. In the last 20 hours where the motor bearing is in fault state,

the correlation dimension goes around 2.44. And the related deviation is 3%.

Observations from this experiment can be summarized as follows: The shaft current has effect on the correlation dimension of dynamic system. Experiments both based on vibration and current signal analysis cannot detect fault immediately after current injected. That's because bearing fault is not significant. The algorithm works after some hours when the fault becomes significant. Moreover, the result comes from current signal analysis is less significant than that from vibration signal analysis.

B. Induction Motor 3KX07G Loaded by a Generator

In this experiment, a 7.5HP, 3 Phase, 208V bigger induction motor 3KX07G manufactured by DAYTON was used for test. A synchronous generator was used to load the induction motor. To testify the algorithm mentioned in Chapter III, both health and fault signal data are needed. To be different from the G563 motor experiment where bearing was damaged continuously, in this experiment bearing is damaged by step by step. It is conducted as follows: (1) the test-bed is run for about 60 hours over a period of 2.5 days to collect healthy vibration and electric data; (2) inject the shaft current, around 12 A, for around 5 hours in order to damage bearing. This procedure is to generate roughness bearing fault so that the performance of load side bearing deviate from the healthy range; (3) remove the shaft current and collect some hours fault data; (4) repeat step 2 and step 3 to generate the 2nd section of fault data; (5) repeat step 4 to generate the 3rd section of fault data.

1. Vibration Signal Analysis

The sampling rate of vibration signal is set at 12.8 kHz. Each data file is recorded by LabView on PC every minute. It contains one minute length signal. Before data being applied in fault detection, threshold de-noising method based on wavelet is used for filtering background noise. The detail setting for de-noising is shown as follows. Select the db30 wavelet, level 8, entropy type sure, and threshold parameter 2.0 based on soft threshold algorithm. However, it is very time consuming if all the sampled data is used for correlation dimension calculation. Thus, 10K points (about 9 seconds) data is applied to the algorithm to represent whole minute.

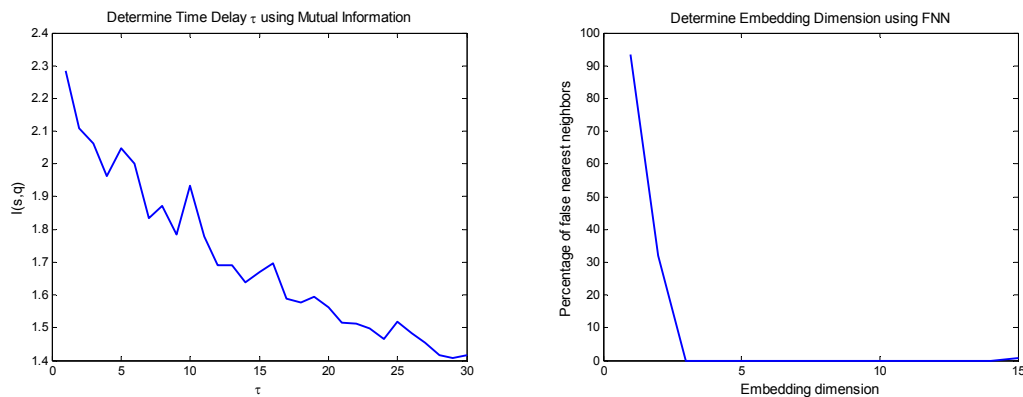


Figure 38. Average mutual information and embedding dimension.

To reconstruct the phase space, two important parameters, time delay and embedding dimension need to be determined. Referring to Figure 38, a time lag of 4 is appropriate and an embedding dimension of 12 is sufficient.

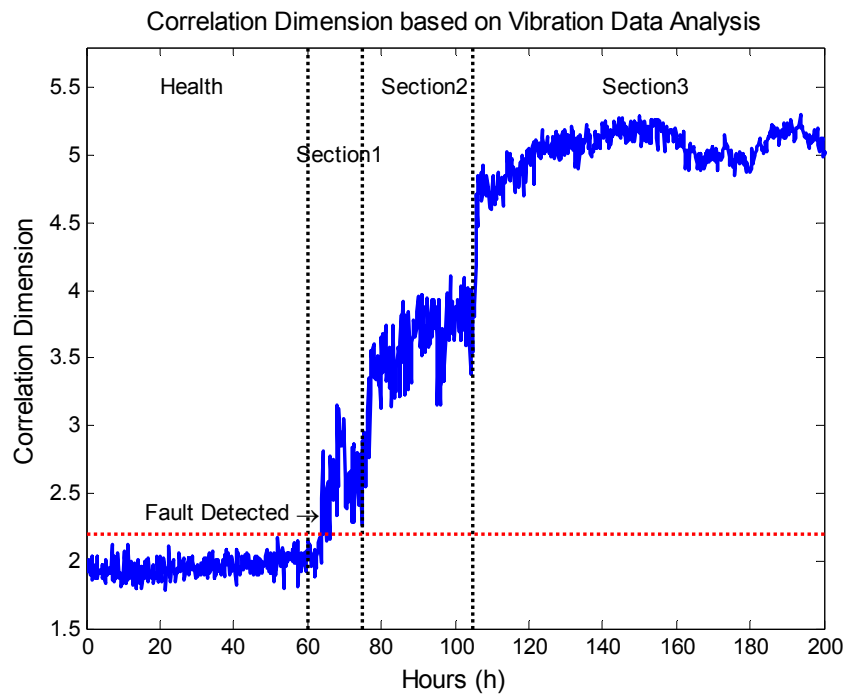


Figure 39. Correlation dimension based on vibration data analysis.

The result of second experiment based on vibration signal analysis is shown in Figure 39. In this experiment, the values of correlation dimension never go higher than 2.2 in first 60 hours where the bearing of motor can be seen as health. The shaft current is injected at about 60th hour after the experiment started. The correlation dimension is rising because the bearing is damaged. The value of threshold is set at 2.2. The bearing fault can be detected at 65th hour. Moreover, three sections can be clearly seen in figure. The correlation dimensions of three different fault sections are distributed in three separately range. In the last 50 hours where the motor bearing is in fault state, the correlation dimension goes around 5. And the related deviation is 150%.

2. Current Signal Analysis

The sampling rate of electric signal is set at 8 kHz. It is sampled by AD converter and then transferred by BF537 to PC every 30 seconds. To reduce computational time, resample the signal from 8kHz to 19.2kHz and just use one data file set to the algorithm to represent ten minutes. Moreover, before current data is applied in fault detection, filter bank based on wavelet is used for filtering harmonic frequencies.

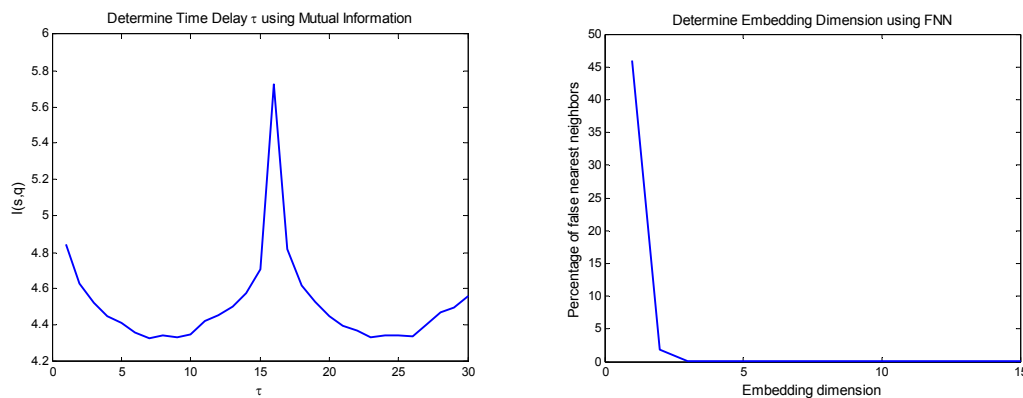


Figure 40. Average mutual information and embedding dimension.

To reconstruct the phase space, two important parameters, time delay and embedding dimension need to be determined. Referring to Figure 40, a time lag of 8 is appropriate and an embedding dimension of 10 is sufficient.

The result of second experiment based on current signal analysis is shown in Figure 41. In this experiment, the values of correlation dimension never go higher than 1.75 in first 60 hours where the bearing of motor can be seen as health. The shaft current is injected at about 60th hour after the experiment started. The value of threshold can be set

at 1.75. The correlation dimension is rising a little in 1st section because the bearing is slightly damaged. The correlation dimension in the 2nd section changes significantly. The bearing fault can be detected at about 80th hour. In the last 50 hours where the motor bearing is in 3rd fault state, the correlation dimension goes around 1.82. And the related deviation is 6%.

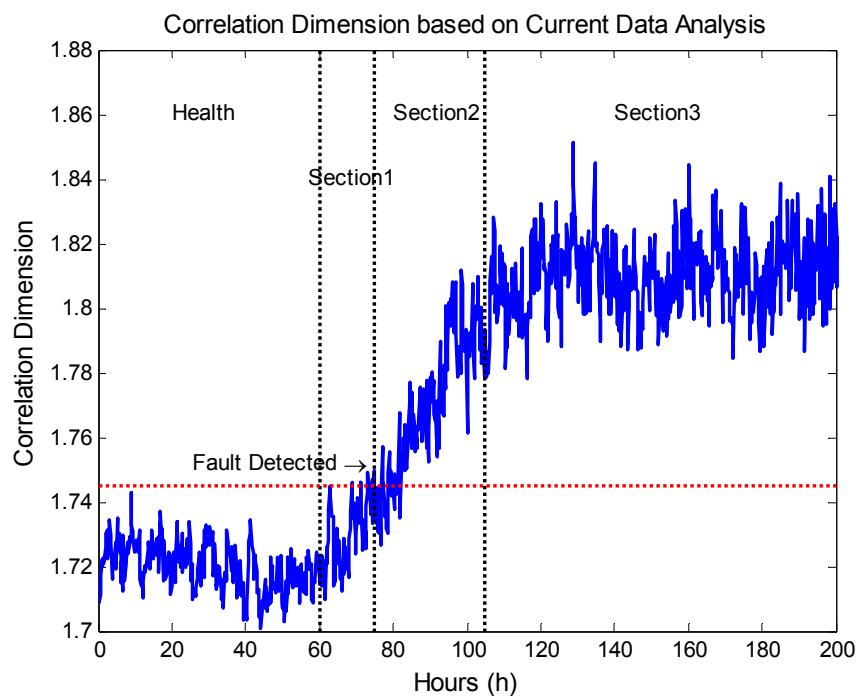


Figure 41. Correlation dimension based on current data analysis.

Observations from this experiment can be summarized as follows: The shaft current has effect on the correlation dimension of dynamic system. Experiments both based on vibration and current signal analysis cannot detect fault immediately after current injected. That's because bearing fault is not significant. The algorithm based on vibration

data analysis is more sensitive than that based on current signal, and three sections can be clearly seen in Figure 39. Thus it is more applicable for slight bearing fault detection. Moreover, the result comes from vibration signal analysis is more significant. However, it has been proved that stator current monitoring can detect bearing fault successfully without requiring access to the motor. Though the result from current-based monitoring technique is not sensitive as vibration signal, it usually does not require additional sensors (sensorless) so that it is inexpensive and has great economic benefit for low-cost implementations.

C. An Extended Application

To justify the extended application of detecting other than bearing faults, the algorithm is also applied to a set of field data. An application of motor pump system undergoing a pump seal failure (leak) is considered. In this test which is shown in Figure 42, the values of correlation dimension never go higher than 1.61 in the first 45 days when the motor can be seen as health. The correlation dimension starts rising at the about 45th day after the monitoring period started. The value of threshold is set at 1.61. The fault can be first detected on the 50th day as shown in the following figure. After 60th day, the correlation dimension significantly deviates from the range of health state. Therefore, this algorithm has the potential to detect other faults beyond bearing faults.

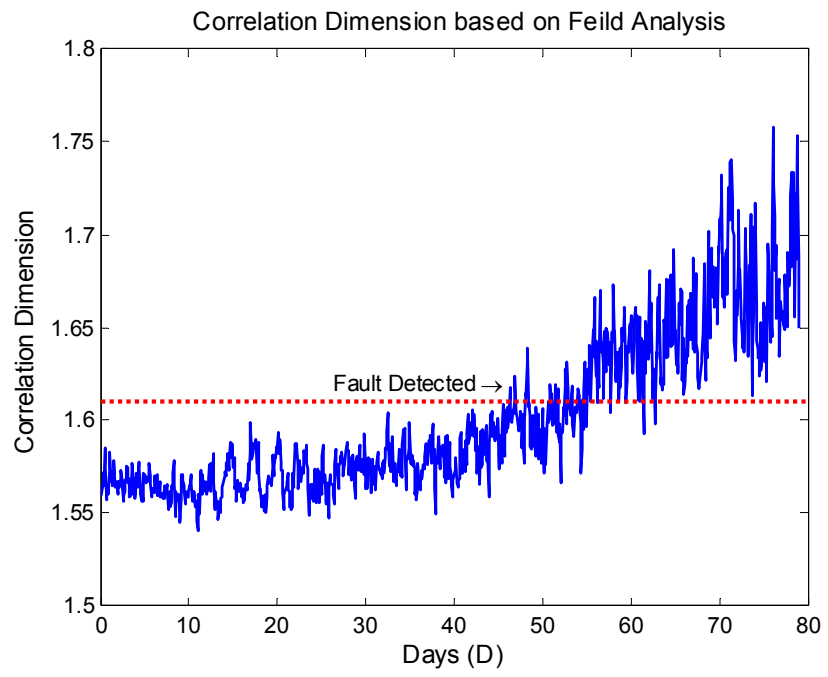


Figure 42. Correlation dimension based on field analysis.

CHAPTER V

SUMMARY AND CONCLUSIONS

In this chapter, the work of this research is summarized. The main objective of this thesis was to study the induction motor bearing faults and find out a new method for detecting roughness faults. The result of research is discussed and some suggestions for future work are given.

A. Summary of Research

Fault detection is a very important research area in mechanical engineering studying. Because bearing failures can be considered the most common failures of motors, there is a strong motivation to study bearing faults and develop a method for detecting faults in induction motor.

All faults related to bearing can be categorized into single-point defects or generalized roughness defects. In many research, monitoring methods based on vibration signals are used to detect the single-point bearing failure. Depending on which bearing surface contains the fault, the characteristic vibration frequencies, can be calculated from the rotor speed and the bearing geometry. It also has been proved by Schoen and Habetler that stator current monitoring can provide the same indications without requiring access to the motor. In the contrast to single-point defect, generalized roughness work is needed to investigate exact effects.

The combination of phase space reconstruction technology and fractal theory can

provide an effective method to detect bearing generalized roughness faults in induction motor.

In mathematics, a delay embedding theorem gives the conditions under which a chaotic dynamical system can be reconstructed from a sequence of observations of the state of a dynamical system by lagging the time series to embed it in more dimensions. There are two steps to reconstructing phase space from a signal: first step is choosing a time delay; second step is choosing an embedding dimension. One can determine of delay time by calculating mutual information with equality distant space cells. That means space cells are divided by equal distance step for calculating mutual information, and delay time. This approach is simpler than that of equal probability method. False nearest neighbors provides a robust way to determine necessary embedding dimensions. The basic idea of False nearest neighbor is: “two points which are close in the reconstructed state space stay close under forward iteration.”

Almost all chaotic systems have a quantifying measurement known as a fractal dimension which is extracted from the original or reconstructed phase space and applied to speech recognition or classification. There are many specific forms of fractal dimension. Similarity dimension directly comes from the definition of fractal dimension, it is easiest to be understood and computed. Generally none real-world object or shape has clearly repeating self-similar structure as Sierpinski triangle and Koch curve. It means that the similarity dimension algorithm will not work because real-world objects have less regular shapes and cannot be divided into equal segments. In such cases box-counting dimension is more widely used, which is often based on calculating

occupied boxes algorithm. However, the phase spaces are usually high dimension Euclidean space. When dimension goes higher and higher, the algorithmic complexity grows exponentially with the set dimension, calculating box-counting dimension require a prohibitive amount of computation time. Thus, the box-counting dimension can be computed only for low-dimensional sets. Therefore, correlation dimension is a good substitute for the box-counting dimension due to its computational simplicity. It can be successfully used to estimate the dimension of attractors of dynamical systems.

Not only the embedding dimension and the lag time but also the data length and the noise level are important factor that influences the computational precision significantly. As is well-known, signals are inevitably corrupted with various types of noise. So it is necessary to eliminate noise before using G-P algorithm to calculate the correlation dimension.

In order to justify this bearing fault detection method, not only bearing health data but also fault data must be acquired before being applied in prognosis. Moreover, it is demonstrated in that the act of this process significantly alters the current and vibration characteristics of the machine and corrupts the experimental data. It is invalid for use in bearing condition monitoring scheme. In the research where data came from, shaft current bearing damage experiments was conducted to induce and progress a bearing fault in an accelerated timeframe. These faults were generated in situ without disrupting the operation of the electric machine.

B. Conclusions

The conclusions drawn from this research are summarized as follows:

1. The algorithm based on vibration and current signal analysis can both detect bearing roughness faults successfully, then experimental and practical results show that the bearing fault detection rate is 100% and there are no false alarms.

2. Experiments both based on vibration and current signal analysis cannot detect fault immediately after current injected. That's because bearing fault is not significant. The algorithm works after some hours when the bearing becomes worse. Moreover, the result comes from current signal analysis is less significant than that from vibration signal analysis.

3. Though the result from current-based monitoring technique is not sensitive as vibration signal, it usually does not require additional sensors (sensorless) so that it is inexpensive and has great economic benefit for low-cost implementations.

4. In the contrast to the existing sensorless techniques, the phase space reconstruction technology and fractal theory do not require thorough knowledge of stator current spectrum distribution as well as the frequencies of non-bearing fault component.

C. Suggestions for Future Work

The fault detection method developed in this research has proven to be a viable tool to detect rolling element bearing generalized roughness faults. Based on the research reported in this thesis, there are some important questions regarding to these issues that remain unanswered and are given as suggestions for future work. These questions that

require more research are listed below:

1. Irregular embeddings - The methods to estimate d_e and r described in the previous sections assume that a single embedding lag is sufficient. Often, one encounters dynamical system where the important variables are different in different parts of phase space. Another way of describing this is to say that the embedding is not constant. It has been demonstrated that variable embeddings behave quantitatively better than uniform embeddings. These problems can be considered in more detail in future.

2. Lyapunov exponents - The thesis have been discussing the estimation of dynamic invariants and have introduced the fractal dimension. There is another type of dynamic invariant: invariants related to the dynamic evolution of attractor. These invariants are typically measure of Lyapunov exponents that also can be applied to fault detection.

3. Other phases signal - Based on phase space reconstruction technology, just one phase current signal is used for analysis to get the correlation dimension of system. However, the electric data acquisition can get three phases signal. How to use the other two channels data is needed to investigate more effects.

4. Load independence – The experiments in this research did not change the load of all motors. An ideal method should be load independent so that it will be more applicable for practical analysis. To justify the load effects of the bearing fault detection method is one of the topics for future research.

5. Other types of motor faults – Though bearing failures are considered the most common failures of electric motors. Stator, rotor, and other failures cannot be ignored. Further research on other types of motor fault detection is needed in order to distinguish

the bearing faults from other types of motor faults.

REFERENCES

- [1] A. K. S. Jardine, D. Lin, and D. Banjevic, "A review on machinery diagnostics and prognostics implementing condition-based maintenance," *Mechanical Systems and Signal Processing*, vol. 20, no. 7, pp.1483–1510, Oct. 2006.
- [2] P. O'Donnell, "Report of large motor reliability survey of industrial and commercial installations: Part I and II," *IEEE Trans. Ind. Appl.*, vol. IA-21, no. 4, pp. 853–872, Jul./Aug. 1985.
- [3] P. F. Albrecht, J. C. Appiarius, and D. K. Sharma, "Assessment of reliability of motors in utility applications—Updated," *IEEE Trans. Energy Convers.*, vol. EC-1, no. 1, pp. 39–46, Mar. 1986.
- [4] O. V. Thorsen and M. Dalva, "A survey of faults on induction motors in offshore oil industry, petrochemical industry, gas terminals, and oil refineries," *IEEE Trans. Ind. Appl.*, vol. 31, no. 5, pp. 1186–1196, Sep./Oct. 1995.
- [5] K. Singh and S. A. S. Al Kazzaz, "Induction machine drive condition monitoring and diagnostic research - a survey," *Electric Power Systems Research*, vol. 64, no. 2, pp. 145–158, Feb. 2003.
- [6] J. Stack, T. G. Habetler, and R. G. Harley, "Fault classification and fault signature production for rolling element bearings in electric machines," *IEEE Trans. Ind. Appl.*, vol. 40, no. 3, pp. 735–739, May/Jun. 2004.
- [7] R. R. Schoen, T. G. Habetler, F. Kamran, and R. Bartheld, "Motor bearing damage detection using stator current monitoring," *IEEE Trans. Ind. Appl.*, vol. 31, no. 6, pp. 1274–1279, Nov./Dec. 1995.
- [8] B. Yazici and G. B. Kliman, "An adaptive statistical time–frequency method for detection of broken bars and bearing faults in motors using stator current," *IEEE Trans. Ind. Appl.*, vol. 35, no. 2, pp. 442–452, Mar./Apr. 1999.
- [9] L. Eren and M. J. Devaney, "Bearing damage detection via wavelet packet decomposition of the stator current," *IEEE Trans. Instrum. Meas.*, vol. 53, no. 2, pp. 431–436, Apr. 2004.
- [10] J. Stack, T. G. Habetler, and R. G. Harley, "Bearing fault detection via autoregressive stator current modeling," *IEEE Trans. Ind. Appl.*, vol. 40, no. 3, pp. 740–747, May/Jun. 2004.
- [11] L. Wang, "Induction motor bearing fault detection using a sensorless approach,"

Ph.D. dissertation, Dept. Mech. Eng., Texas A&M Univ., College Station, TX, 2007.

[12] C. -H. Chen, R. -J. Shyu, and C. -K. Ma, "Rotating machinery diagnosis using wavelet packets-fractal technology and neural networks," *Journal of Mechanical Science and Technology*, vol.21, no. 7 pp.1058-1065, Nov. 2007.

[13] D. Logan and J. Mathew, "Using the correlation dimension for vibration fault diagnosis of rolling element bearing - 2. Selection of experimental parameters," *Mechanical Systems and Signal Processing*, vol. 10, no. 3, pp. 251-264, May 1996.

[14] J. R. Stack, T. G. Habetler, and R. G. Harley, "Experimentally generating faults in rolling element bearings via shaft current," *IEEE Trans. Ind. Appl.*, vol. 41, no. 1, pp. 25-29, Jan./Feb. 2005.

[15] A. C. Lindgren, M. T. Johnson, and R. J. Povinelli, "Speech recognition using reconstructed phase space features," in *Proc. Int. Conf. Acoustics, Speech, Signal Processing*, Hong Kong, 2003, pp. 61-63.

[16] F. Takens, "Detecting strange attractors in turbulence," (Lecture Notes in Mathematics). *Dyn. Syst. Turbulence*, vol. 898, pp. 366-381, 1981.

[17] E. Ott, W.D. Withers, and J.A. Yorke. "Is the dimension of chaotic attractors invariant under coordinate changes?" *Journal of Statistical Physics*, vol. 36, no. 5-6, pp. 687-697, Sep. 1984.

[18] M. Pannuri. Mutual information and dimension estimation, (Seminars). *IES Spring'06 Seminar Series*, February 16, 2006.

[19] Z. Yang, G. Wang, and S. Chen "Determine of delay time by calculating mutual information with equality distant space cells," *Chinese Journal of Computational Physics*, vol. 12, no. 4, pp. 442-448, Dec. 1995.

[20] A. M. Fraser and H. L. Swinney, "Independent coordinates for strange attractors from mutual information," *Phys. Rev. A, Gen. Phys.*, vol. 33, no. 2, pp. 1134-1140, Feb. 1986.

[21] M. Small, *Applied Nonlinear Time Series Analysis: Applications in Physics, Physiology and Finance*. Singapore: World Scientific, 2005.

[22] Y. Pan and S. A. Billings, "Neighborhood detection for the identification of spatiotemporal systems," *IEEE Trans. Syst., Man, Cybern. B, Cybern.*, vol. 38, no. 3, pp. 846-854, Jun. 2008.

[23] K. Mandli. (2005 June 2). Finding embedding dimensions of chaotic time series

(Presentation for AMATH 575). Available: <http://www.amath.washington.edu/~mandli/>

[24] C. Rhodes and M. Morari, “The false nearest neighbors algorithm: An overview,” *Comput. Chem. Eng.*, vol. 21, Supplement 1, pp. S1149–S1154, May 1997.

[25] B.B. Mandelbrot, *The Fractal Geometry of Nature*. San Francisco, CA: Freeman, 1982.

[26] L. S. Liebovitch and Lina A. Shehadeh. (2005). Introduction to fractals (pdf) in *Tutorials in Contemporary Nonlinear Methods for the Behavioral Sciences* Web Book Eds. M. A. Riley and G. V. Orden, National Science Foundation, Directorate for Social, Behavioral and Economic Sciences. Available: <http://www.ccs.fau.edu/~liebovitch/larry.html>

[27] B. Mandelbrot, “How long is the coast of Britain? Statistical self-similarity and fractional dimension,” *Science*, vol. 156, no. 3775, pp. 636 – 638, May 1967.

[28] E. Lorenz, “Fractals and fractal architecture,” M.S. Thesis, Dept. Computeraided Planning and Architecture, Vienna University of Technology, Vienna, Austria, 2003.

[29] S. Sutherland. (2002, Summer). Mathematical Problem Solving with Computers (Notes for MAT 331). Available: <http://www.math.sunysb.edu/~scott/>

[30] F. Camastra and A. Vinciarelli, “Estimating the intrinsic dimension of data with a fractal-based method,” *IEEE Trans. Pattern Anal. Machine Intell.*, vol. 24, no. 10, pp. 1404–1407, Oct. 2002.

[31] W.J. Wang, J. Chen, J.D. Jiang, and Z.T. Wu, “The application of correlation dimension in large rotating machinery fault diagnosis,” *Journal of Mechanical Engineering Science*, vol. 214, no.7, pp. 921-929, Jul. 2000.

[32] E. N. Lorenz, “Deterministic nonperiodic flow,” *J. Atmosph. Sc.*, vol. 20, pp. 130–141, Mar. 1963.

[33] R. Pravitha, P. Indic, and V. P. N. Nampoori, “Dynamical aspects of coupled Rossler systems: effects of noise,” *Physics Letters A*, vol. 294, no. 1, pp.37-46, Feb. 2002.

VITA

Jianxi Fu received his Bachelor of Science degree from Tsinghua University at Beijing, P.R. China in 2005. He entered the mechanical engineering program at Texas A&M University in September 2008 and received his Master of Science degree in December 2010. His research interests include signal processing, induction motor fault detection and diagnosis, artificial intelligence techniques, and dynamic system estimation and control.

Mr. Fu may be reached at Department of Mechanical Engineering, Texas A&M University, College Station, TX 77843-3123. His email address is fujianxi@tamu.edu or fujianxi@gmail.com.